

**Two-dimensional organic-inorganic superlattice-like heterostructures for energy storage applications**

Journal:	<i>Energy & Environmental Science</i>
Manuscript ID	EE-MRV-10-2020-003206.R1
Article Type:	Minireview
Date Submitted by the Author:	31-Oct-2020
Complete List of Authors:	Xiong, Pan; Nanjing University of Science and Technology Wu, Yunyan; Nanjing University of Science and Technology Liu, Yifan; Nanjing University of Science and Technology Ma, Renzhi; National Institute for Materials Science, Soft Chemistry Group, Advanced Materials Laboratory Wang, Xin; Nanjing University of Science and Technology, Zhu, Junwu; Nanjing University of Science & Technology Sasaki, Takayoshi; National Institute of Materials Science, International Center for Materials Nanoarchitectonics

Two-dimensional organic-inorganic superlattice-like heterostructures for energy storage applications

Pan Xiong^a, Yunyan Wu^a, Yifan Liu^a, Renzhi Ma^b, Takayoshi Sasaki^{b*}, Xin Wang^a, Junwu Zhu^{a*}

^aKey Laboratory for Soft Chemistry and Functional Materials of Ministry Education, Nanjing University of Science and Technology, Nanjing, 210094, China

^bInternational Center for Materials Nanoarchitectonics (WPI-MANA), National Institute for Materials Science (NIMS), Namiki 1-1, Tsukuba, Ibaraki, 305-0044, Japan

*Corresponding authors

Email: sasaki.takayoshi@nims.go.jp (T.S.); zhujw@njust.edu.cn (J.Z.)

Abstract

Two-dimensional (2D) superlattices, assembled by vertically stacked inorganic 2D nanosheets, are a new class of artificial 2D materials of significant scientific and technological importance. The incorporation of an infinite number of organic molecules within these systems further provides unlimited possibilities for the design and synthesis of 2D organic-inorganic hybrid superlattices with predictable functionalities. Herein, the recent research progress on 2D organic-inorganic hybrid superlattices is summarized. Many facile strategies have been developed for the fabrication of 2D organic-inorganic hybrid superlattices, in which continuous organic layers are intercalated in the interlayer galleries of inorganic 2D nanosheets at an atomic/molecular scale. The advantages of these 2D superlattices are discussed for some typical energy storage applications, such as supercapacitors, lithium/sodium/potassium ion batteries, and multivalent-ion rechargeable batteries. The challenges and perspectives for future researches are also outlined.

1. Introduction

Since the experimental discovery of graphene,¹ great progress has been made on the isolation of two-dimensional (2D) materials. A number of 2D atomic sheets with similar 2D features have been explored by exfoliation of their layered bulk materials, including boron nitride,² transition metal dichalcogenides,³ layered transition metal oxides, and double hydroxides,⁴⁻⁶ transition metal carbides, nitrides and carbonitrides (MXenes),⁷ etc. These 2D nanosheets share an atomic thickness down to the limit of a single layer.^{8,9} Meanwhile, the different chemical composition and crystal structure render them with a wide range of various electronic, optical, and magnetic properties.¹⁰⁻¹⁴ Inspired by the variety of properties, more attention has been recently paid to assemble vertically stacked artificial architecture by using these 2D nanosheets as building blocks, known as 2D heterostructures or superlattices.¹⁵⁻¹⁹ Although the resulting 2D heterostructures and superlattices show a layered structure analogous to that of bulk layered structures and other layered systems, the periodic alternate stacking of dissimilar materials demonstrated fundamental difference.²⁰ Therefore, based on these artificial 2D heterostructures/superlattices, numerous unconventional properties have been demonstrated.^{18,21-26}

Compared to inorganic 2D materials, the molecular design of organic molecules/polymers is much more feasible, resulting in an almost unlimited number of potentially available organic materials with designed functional groups.^{27,28} Recently, these organic materials have been assembled with inorganic 2D materials layer-by-layer into 2D organic-inorganic superlattices.²⁹⁻³¹ The introduction of the chemical tunability of the organic materials to 2D superlattices will result in a possibility to design the properties and functionalities at an atomic/molecular level.³²⁻³⁵ Although such hybrid systems can be considered as biphasic composites, where organic and inorganic phases are hybridized at sub-nanometre to nanometre scales, the combination of two different components, at the molecular level, provides a method to design new nanoarchitectures as well as the ability to improve the properties of both components.^{36,37}

One of the main challenges for the 2D organic-inorganic superlattices is to develop a synthesis method that can preserve or enhance the best properties of each component while eliminating or reducing their particular limitations.³⁸ So far, there are several approaches for the synthesis of 2D organic-inorganic superlattices, which can be divided into direct intercalation of polymers, intercalation of monomers and interlayer polymerization, layer-by-layer assembly, and delamination-

reassembly. Through appropriate synthesis strategies, the organic layers could be positioned in the interlayer with controlled orientation. Thus, at the high-quality atomic/molecular interfaces, organic and inorganic materials combine to reinforce or modify each other.^{39,40} Besides, the choice of organic materials is also crucial. Among various organic materials, the conducting polymers are of interest for the development of 2D organic-inorganic superlattices with suitable conductivities for energy storage applications.⁴¹ They are the polymeric ionic conductors that can transport the electrical signals by weakly coordinated ions, such as poly(ethylene oxide) (PEO) and electronically conducting polymers with conjugated bonds in a macromolecule, such as polyaniline (PANI). The synergetic effects between organic and inorganic materials are supposed to endow the 2D organic-inorganic superlattices with promising new properties for applications in many fields including energy storage devices.^{42,43} Recently, conducting polymers-intercalated layered inorganic materials have been intensively investigated due to their potential use as electrode materials in rechargeable batteries.⁴⁴⁻⁴⁷ The introduction of high molecular weight polymers into the interlayer of the layered hosts would improve the cycling stability, which is particularly favorable for the rechargeable battery based on the beyond-Li ions.^{45,48} Although great progress has been achieved recently in the field of 2D organic-inorganic superlattices for energy storage applications, a timely summary has not yet been conducted, to the best of our knowledge.

Herein, we overview recent progress in 2D organic-inorganic superlattices for energy storage applications. We present the synthesis strategies for the fabrication of 2D organic-inorganic superlattices (Figure 1). We then discuss the improved electrochemical performance of these 2D superlattices in some energy storage systems. We also provide an outlook on challenges and perspectives associated with 2D organic-inorganic superlattices for further research.

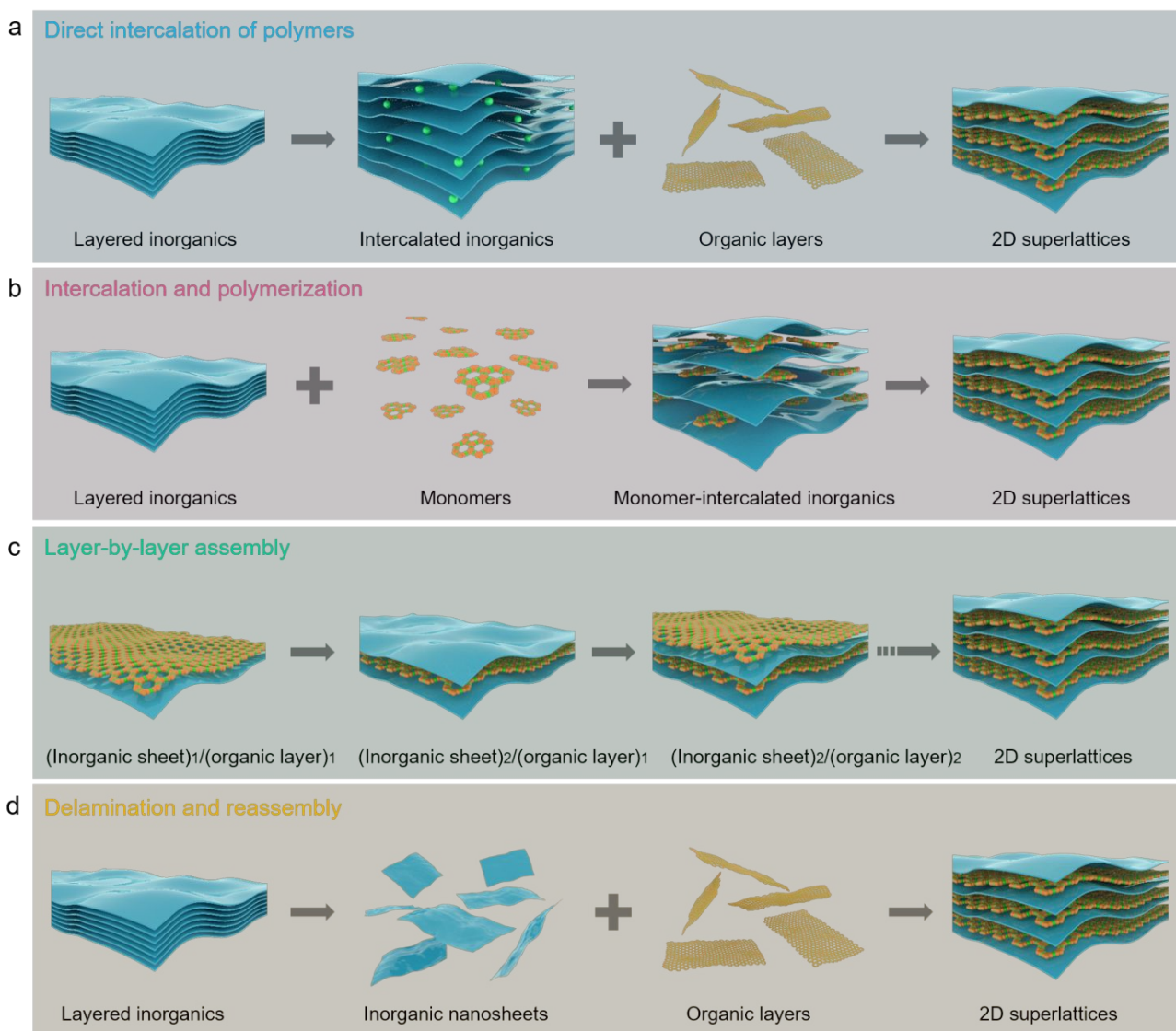


Figure 1. Different synthesis methods for fabrication of 2D organic-inorganic superlattices using inorganic nanosheets and organic layers as building blocks. (a) Direct intercalation of polymer layers into the layered inorganics for the 2D organic-inorganic superlattices. (b) Intercalation of monomers into the layered inorganics and interlayer polymerization for the 2D organic-inorganic superlattices. (c) Layer-by-layer assembly of inorganic sheets and organic layers for the 2D organic-inorganic superlattices. (d) Delamination of layered inorganics into nanosheets and then reassembly of the inorganic nanosheets and organic layers for the 2D organic-inorganic superlattices.

2. Synthesis of 2D organic-inorganic superlattices

Various synthesis strategies have been developed for the fabrication of 2D organic-inorganic superlattices, including direct intercalation of polymers, intercalation of monomers and interlayer polymerization, delamination-reassembly, layer-by-layer (LBL) self-assembly, and “bottom-up” synthesis. Among them, the “bottom-up” synthesis was realized through the in-situ nucleation and

growth of inorganic monolayers on organic molecules/polymer templates,⁴⁹⁻⁵⁷ which requires strict requirements and difficulties in controlling template-mediated anisotropic growth to avoid the formation of bulk inorganic materials and phase separation between inorganic and organic. In contrast, the other four approaches are simple and efficient strategies for cost-effective and scalable synthesis. In this section, the direct intercalation of polymers, intercalation of monomers and interlayer polymerization, delamination-reassembly, and LBL self-assembly will be mainly discussed for the synthesis of 2D organic-inorganic superlattices.

2.1 Direct intercalation of polymers

One of the most straightforward methods for the fabrication of 2D organic-inorganic superlattices is the direct intercalation of polymers into the interlayers of inorganic layered hosts. For example, polyaniline (PANI)-intercalated graphite oxides (GOs), FeOCl, or layered MnO₂ heterostructures had been synthesized via exchange reaction of PANI with alkylamine-intercalated GOs, FeOCl, or MnO₂ in an organic solvent, respectively.^{58,59} By changing the contents of alkylamine in the starting materials, the content of intercalated PANI and the interlayer spacings varied. Based on the basal spacing of the resulting PANI-MnO₂, Zhang et al. found that the benzene rings of PANI were arranged in a zigzag conformation and located perpendicular to MnO₂ layers.⁵⁹ Recently, Yang's group reported the direct intercalation of polymer (polyethyleneimine, PEI) molecules into the interlayers of prepared MoS₂ multilayered crystallites by mixing the NH₄⁺-intercalated MoS₂ with PEI at room temperature (Figure 2a).⁴⁸ The direct intercalation was induced by the strong electrostatic interaction between the positively charged NH₂⁺ groups of PEI and negatively charged MoS₂ nanosheets. As a result, an increased *d*-spacing of (002) plane for the MoS₂-PEI composite was observed, suggesting the intercalation of PEI molecules into the MoS₂ interlayers (Figure 2b). They further studied the direct intercalation of polymers within 2D layered materials by ab initio molecular dynamics (AIMD) calculations. The simulated configurations of PEI-intercalated MoS₂ in an initially ordered state and a final relaxed state both gave an interlayer distance of 10.8 Å (Figure 2c and d), agreeing with the experimental value. The diffusion process of the PEI polymers intercalating into MoS₂ interlayers was further simulated (Figure 2e-h). At the initial state, a PEI molecule was placed outside near the MoS₂ layers. Then, the PEI molecule adsorbed on the MoS₂ edge by attaching the NH₂⁺ group to the sulfur site of MoS₂. After that, the PEI molecule started to intercalate into MoS₂ layers. Eventually, the PEI molecule fully

entered the interlayer galleries.

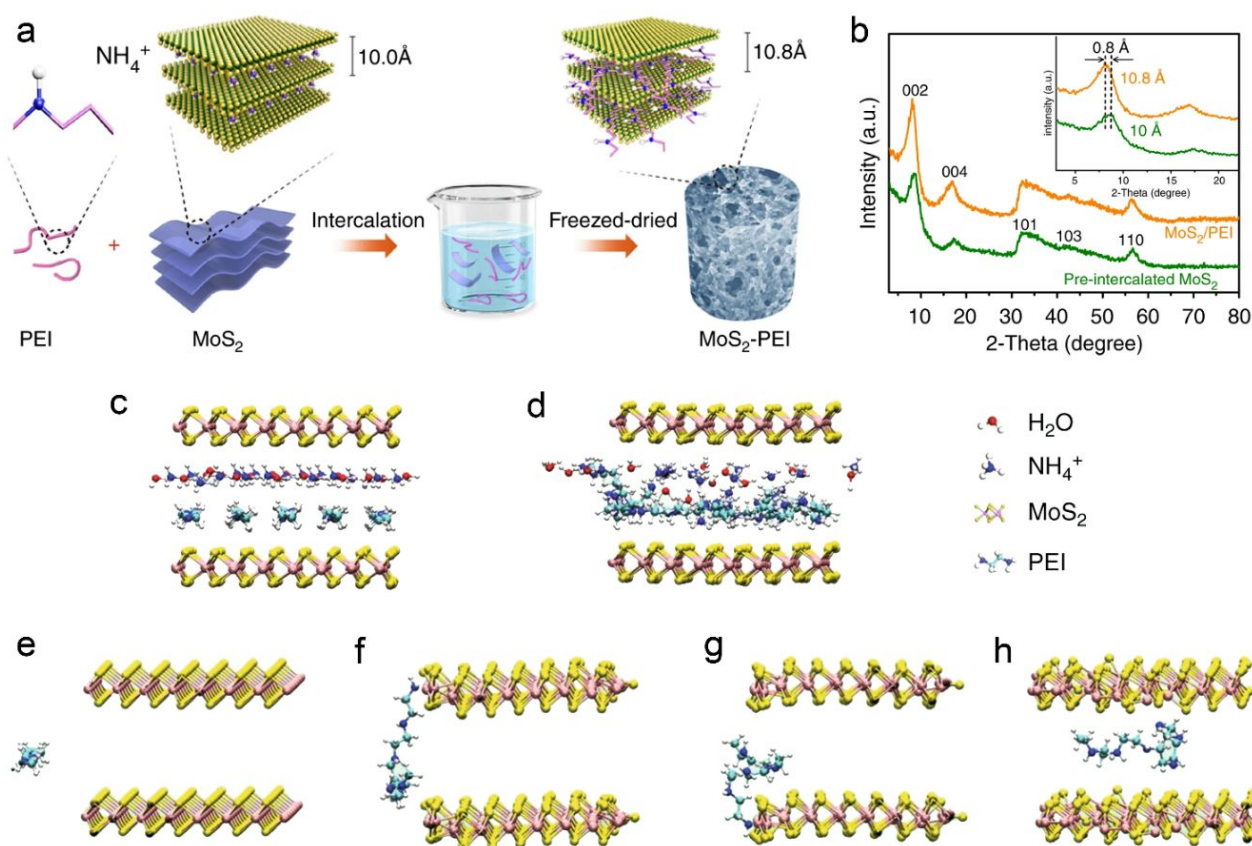


Figure 2. Fabrication of 2D organic-inorganic superlattices by direct intercalation of polymers into the interlayers of layered inorganics. (a) The schematic illustration for the synthetic procedure of the MoS₂-PEI heterostructures. (b) X-ray diffraction (XRD) patterns of the MoS₂ multilayered crystallites and MoS₂-PEI composite. (c-h) Molecular dynamics calculations of the diffusion process of the polymers intercalating into MoS₂ nanosheets. (c and d) Schematic illustration shows configurations of PEI-intercalated MoS₂ with the resulted interlayer distance of 10.8 Å: (c) an initially ordered state; (d) the final relaxed state. (e-h) Illustration of PEI molecule intercalation process with the MoS₂ interlayer distance of 10 Å: (e) 0 ps, (f) 4 ps, (g) 6 ps, and (h) 7 ps. Reproduced with permission.⁴⁸ Copyright 2019, Nature Publishing Group.

2.2 Intercalation of monomers and interlayer polymerization

In addition to the direct intercalation of polymers, the intercalation of monomers and interlayer polymerization is another efficient method for the fabrication of 2D organic-inorganic superlattices. By intercalation of monomers into layered inorganic materials followed by polymerization between the layers with different methods, two distinct chemical components, the organic and inorganic materials, can be hybridized at a molecular level.

Oxidative polymerization of monomer in the interlayer spacing of the layered host is the most direct method.⁶⁰⁻⁶³ In this case, the host materials should possess a strong oxidizing layer that provides

the driving force for the insertion of the monomers into the inorganic galleries and then the oxidative interlayer polymerization of the monomers. Thus, the layered host materials that possess redox couples are usually used, such as V_2O_5 , $FeOCl$, and $VOPO_4$. Taking $V_2O_5/PANI$ as an example, the mechanism of the oxidative polymerization process of aniline monomers in the interlayer spacing of V_2O_5 was investigated.^{64,65} The aniline monomers were first converted to anilinium cations in an acidic environment. The V_2O_5 shows a high affinity for nitrogenated compounds because of its Brønsted-acid character.⁶⁶ Then, the anilinium cations could diffuse into the interlayer space of V_2O_5 due to an acid-base interaction. The intercalated anilinium cations were subjected to oxidative polymerization, during which the layered V_2O_5 was used as an oxidation agent. With the in-situ intercalation and polymerization proceeding, the bulk layered V_2O_5 was exfoliated to form $V_2O_5/PANI$ nanocomposite. Guo et al. reported a similar approach, a silk reeling-like process, for the fabrication of layered hybrid $V_2O_5/poly(3,4\text{-ethylenedioxythiophene})$ ($V_2O_5/PEDOT$) nanowires.⁶⁷ Upon simply mixing V_2O_5 powders and 3,4-ethylenedioxythiophene (EDOT) monomers in aqueous solution, EDOT started to intercalate into the surface layers of V_2O_5 microrods and then polymerized, forming intercalated bilayers of PEDOT between V_2O_5 bilayers. With continuous stirring, the friction between the microrods and the solvent may peel the intercalated surface layers of the microrods to form nanowires, similar to the cocoon-to-silk fiber reeling process (Figure 3a). The morphology characterizations showed the conversion from the microrods to nanowires (Figure 3b-d). After the conversion process, the $V_2O_5/PEDOT$ nanowires showed an interlayer spacing of 18.6 Å (Figure 3e), which is close to the reported value for the interlayer spacing of bilayer V_2O_5 intercalated with bilayers of PEDOT.⁶⁸ Recently, Li's group reported the synthesis of $V_2O_5/PEDOT$ via a simple one-pot self-polymerization method by stirring V_2O_5 powder and EDOT monomer together (Figure 3f).⁴⁶ Similarly, the polymerization of EDOT did not require an additional oxidizing agent; the V_2O_5 itself could serve as the oxidizing agent. EDOT monomers could gradually insert into the interlayers of V_2O_5 , and therein were polymerized into PEDOT, leading to an evident expansion of interlayer spacing (Figure 3g). Xia's group demonstrated the redox intercalative polymerization for the synthesis of PEDOT-intercalated ammonium vanadate oxide (NVO) (Figure 3h).^{45,69} The layered NVO was first produced by sonication treatment of V_2O_5 in $(NH_4)_2S_2O_8$ (APS) solution. After adding the EDOT monomers into the NVO suspension, the polymerization of EDOT monomers and intercalation of just-synthesized

PEDOT into NVO occurred simultaneously, accompanied by a sacrificial reduction of the V_3O_8 layers. High-resolution TEM (HRTEM) images showed an expanded interlayer distance of 10.8 Å for the PEDOT-intercalated NVO than that (7.8 Å) for the pure NVO (Figure 3i and j), suggesting the successful intercalation of PEDOT (Figure 3k).

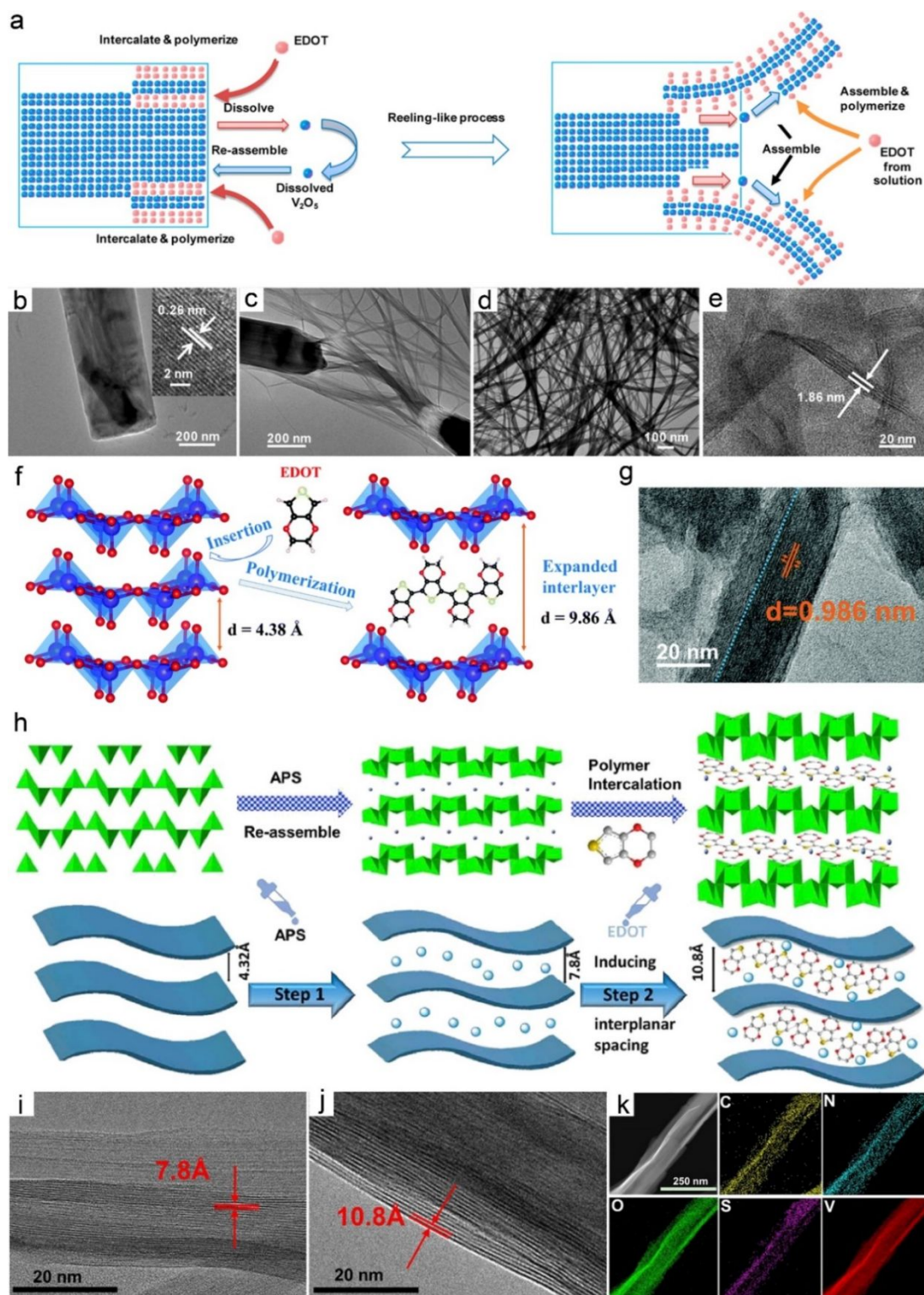


Figure 3. Fabrication of 2D organic-inorganic superlattices by intercalation of monomers and

interlayer polymerization. (a) The schematic illustration for the reel-like process to produce V_2O_5 /PEDOT nanowires from V_2O_5 microrods. (b-e) SEM images showing an EDOT-induced reel-like process to produce layered hybrid V_2O_5 /PEDOT nanowires from V_2O_5 microrods. TEM images of (b) V_2O_5 microrod, (c) intermediate products during the synthesis process, (d) V_2O_5 /PEDOT nanowires and (e) the layered structure of the V_2O_5 /PEDOT nanowires. Reproduced with permission.⁶⁷ Copyright 2015, American Chemical Society. (f) Schematic illustration for the synthesis of V_2O_5 /PEDOT. (g) HRTEM image of the V_2O_5 /PEDOT. Reproduced with permission.⁴⁶ Copyright 2020, The Royal Society of Chemistry. (h) Schematic illustration of the preparation of PEDOT-intercalated NVO layered materials. HRTEM images of (i) NVO and (j) PEDOT-intercalated NVO. (k) Elemental mapping analysis of the PEDOT-intercalated NVO material. Reproduced with permission.⁴⁵ Copyright 2020, Cell press.

The above interlayer polymerization was limited to some redoxable layered host. Oxidative polymerization in the presence of an oxidation reagent or electrochemical method is more widely applied.⁷⁰⁻⁷² Nanocomposites of PANI and different layered protonic transition-metal oxides (HNb_3O_8 , $HTiNbO_5$, and $HSr_2Nb_3O_{10}$) were prepared via the polymerization of monomers within the confined interlamellar space.^{73,74} Aniline monomers were first inserted into the layered protonic transition-metal oxides based on an acid/base reaction. Then, the interlayer polymerization of aniline monomers was initiated by microwave irradiation or chemical oxidants of either $(NH_4)_2S_2O_8$ or $FeCl_3$. Two different mechanisms were proposed for these two different polymerization approaches.⁷³ Since the chemical oxidizing agent cannot easily diffuse into the interlamellar space, the polymerization of aniline started at the edge of the layer with the formation of an anilinium cation radical. Then the cation radical reacted with the aniline monomers and continuously underwent a chain growth reaction to form a high molecular weight polymer into the inner part. For the polymerization by microwave irradiation with penetration character, the aniline monomers within the interlamellar space could be simultaneously excited to form cation radicals. Then, the radicals easily reacted with each other to form oligomers within the limited space, forming PANI molecules with a relatively lower molecular weight.

Electrochemical molecular intercalation has been demonstrated to be an efficient approach to fabricate organic-inorganic superlattices in which monolayer inorganic atomic crystals alternate with organic molecular layers. Wan et al. synthesized inorganic/organic superlattices by electrochemical intercalation of layered transition metal dichalcogenide TiS_2 with organic hexylammonium (HA) cations (Figure 4a).⁷⁵⁻⁷⁷ During the electrochemical intercalation process, the organic cations were intercalated into the van der Waals gap by Coulomb force, and part of the Ti^{4+} in TiS_2 was reduced to

Ti³⁺. High-angle annular dark-field scanning transmission electron microscopy (HAADF-STEM) observations demonstrated that the TiS₂ and organic layers are alternately stacked (Figure 4b and c). This general synthesis route using organic intercalation could be extended to many other layered materials besides the transition metal dichalcogenides. For example, through the similar electrochemical intercalation approach, Duan's group reported a monolayer atomic crystal molecular superlattice (MACMS) consisting of alternating layers of monolayer 2D black phosphorus (BP) atomic crystals and organic cetyl-trimethylammonium bromide (CTAB) molecular layers (Figure 4d).⁷⁸ Cross-sectional TEM images showed an expanded interlayer distance of 11.21 Å, roughly corresponding to the thickness of BP monolayer and end-to-end distance between the CTAB methyl-methyl substituents (Figure 4e and f).

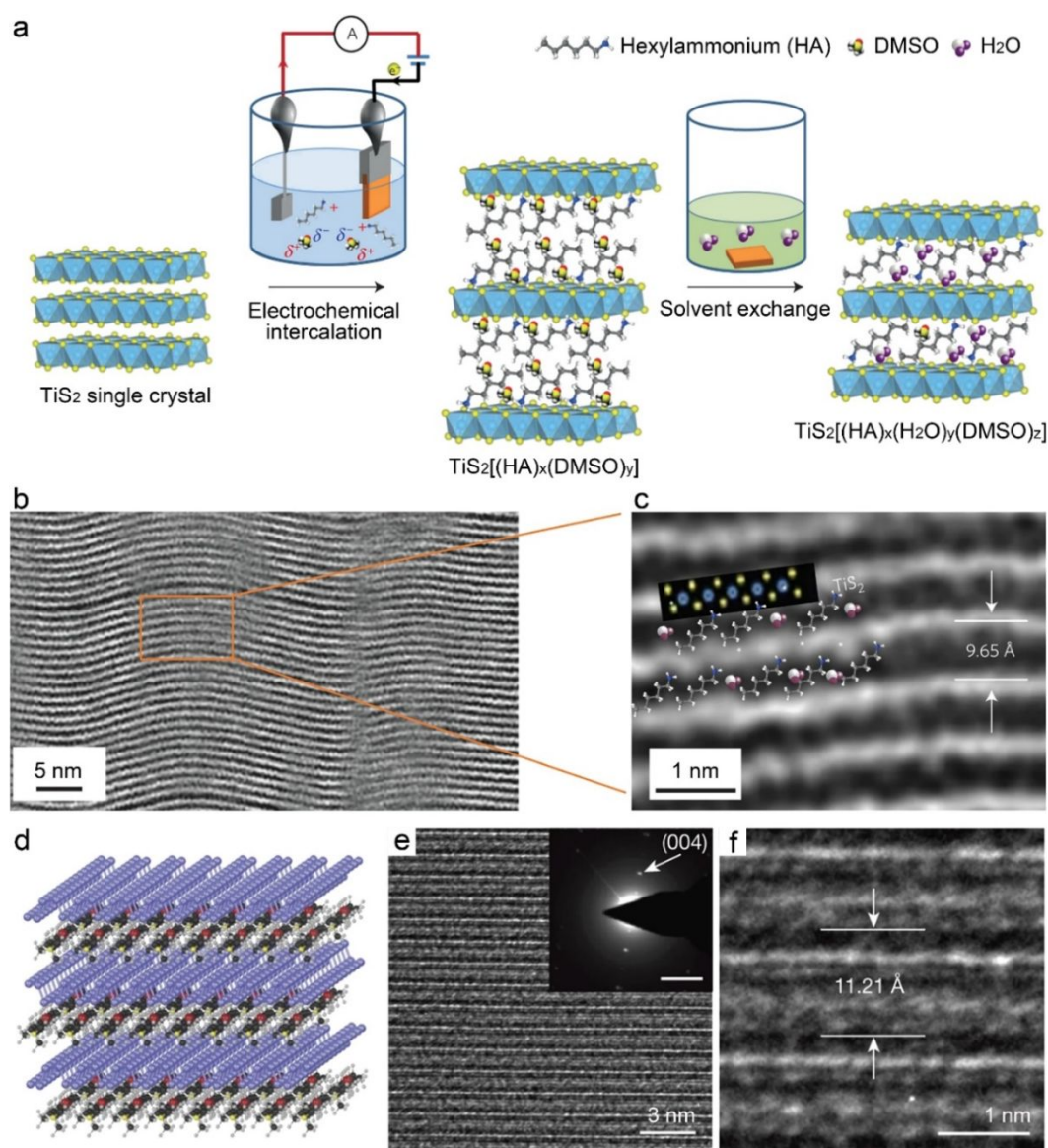


Figure 4. Fabrication of 2D organic-inorganic superlattices by electrochemical molecular

intercalation. (a) The schematic illustration for the synthesis of TiS_2 -based inorganic/organic superlattices. (b) HAADF-STEM image of the $\text{TiS}_2[(\text{HA})_x(\text{H}_2\text{O})_y(\text{DMSO})_z]$ hybrid superlattice showing a wavy structure. (c) Magnified HAADF-STEM image of $\text{TiS}_2[(\text{HA})_x(\text{H}_2\text{O})_y(\text{DMSO})_z]$. Reproduced with permission.⁷⁵ Copyright 2015, Nature Publishing Group. (d) Three-dimensional view of the simulated atomic structure of monolayer phosphorene molecular superlattices (MPMS). (e) Cross-sectional TEM image and (f) high-resolution cross-sectional TEM image of monolayer phosphorene molecular superlattices (MPMS). Reproduced with permission.⁷⁸ Copyright 2018, Nature Publishing Group.

2.3 Layer-by-layer (LBL) assembly

The above methods are based on the intercalation of organic species into the interlayers by a chemical or electrochemical reaction. However, the densely restacked layered architectures with a high charge density or intimate interlayer interaction make it challenging to controllably intercalate bulky guest ions or polymer molecules into the interlayers. Delamination of the multilayered materials into single- or few-layer nanosheets dramatically increases the accessible surface. The synthesis strategies started from the delaminated nanosheets have proven to be an effective and promising route for the synthesis of the organic-inorganic nanocomposite.

The LBL assembly technique is an effective approach for the hybridization of different nanomaterials into an ordered multilayer pattern with desired thickness and designed architecture.⁷⁹⁻⁸² A multilayered organic-inorganic film can be built up by sequential adsorption of nanometer-thick monolayers of oppositely charged inorganic nanosheets and organic polymer ions on a substrate. For example, the LBL assembly of clay nanosheets and polymer chains was used to fabricate clay/polymer composites on different substrates.⁸³⁻⁸⁸ Several groups have demonstrated the fabrication of multilayer ultrathin films incorporating inorganic oxide nanosheets and polymers.⁸⁹⁻⁹⁷ In comparison to the conventional hybrid films produced by in situ intercalation/oxidative polymerization, the LBL films showed maximized interactions between organic and inorganic compounds because of the nanostructured nature of the films, which supposed to enhance the charge storage capability of the hybrid films in comparison to the corresponding individual components.^{95,98} Especially, Sasaki et al. reported a multilayer organic-inorganic superlattice film by sequentially dipping a substrate in a colloidal suspension of negatively charged unilamellar metal oxide nanosheets and an aqueous solution of polycations, such as poly(diallyldimethylammonium chloride) (PDDA) and PEI.^{93,94,99,100} A photograph of the resulting films showed the color change from light brown to deep brown as the

deposition numbers increased (Figure 5a). The linearly increased absorbance (Figure 5b) and XRD peak intensity (Figure 5c) with increasing deposition cycles indicated the successful layer-by-layer assembly of unilamellar metal oxide nanosheets and polycations. In addition to the metal oxide nanosheets, layered organic-inorganic hybrid films of layered double hydroxide (LDH) nanosheets have also been fabricated through the LBL assembly approach.^{101,104} For example, multilayer films of cellulose acetate (CA) and MgAl-LDH nanoplatelets were fabricated by alternately spin-coating of CA and LDH nanoplatelets, followed by thermal annealing treatment (Figure 5d). The (CA/LDH)₂₀ film exhibited high uniformity, flexibility, and transparency (Figure 5e), due to the uniform layered architecture consists of well-dispersed and oriented LDH nanoplatelets within the CA matrix (Figure 5f and g).¹⁰²

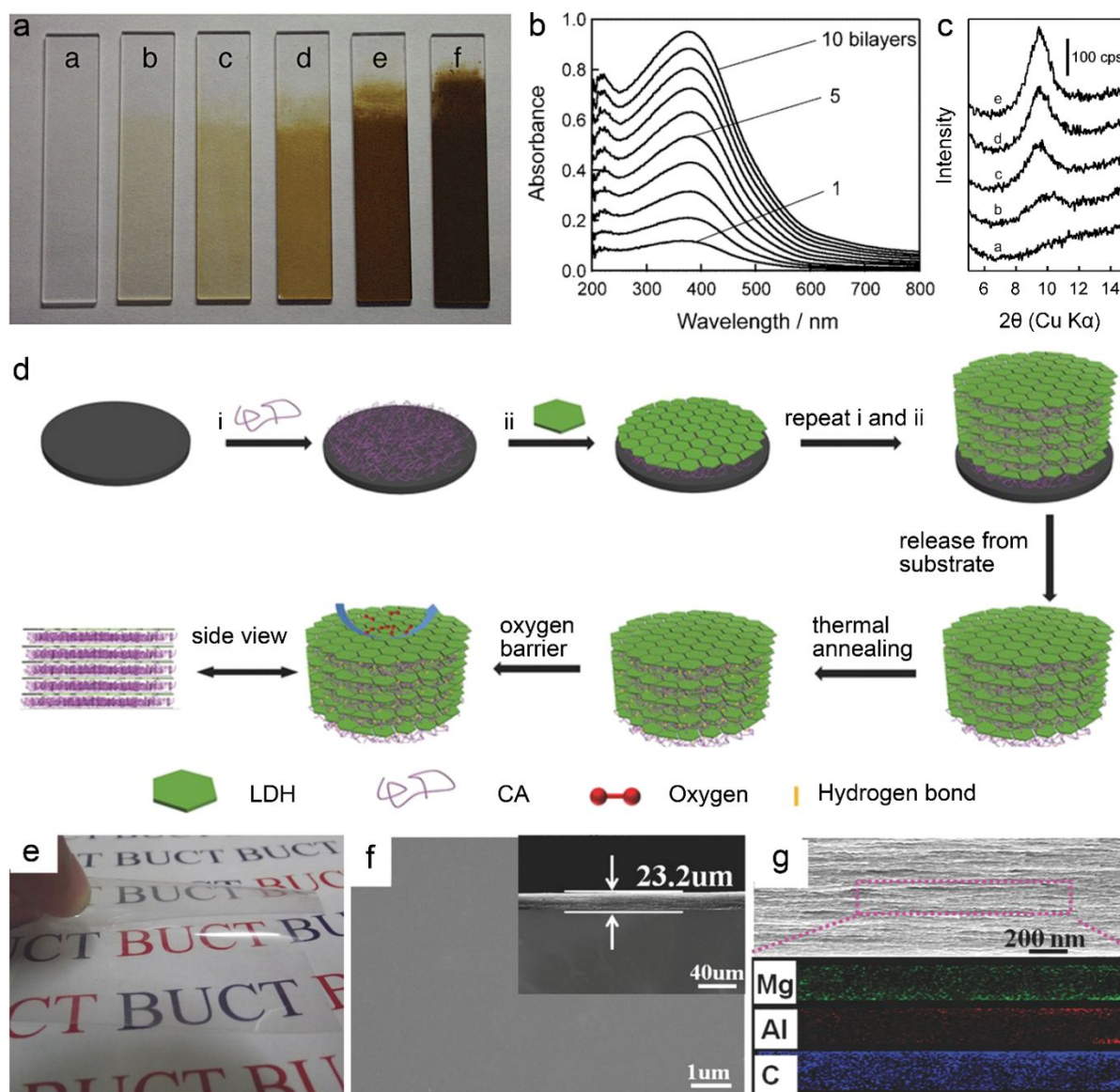


Figure 5. Fabrication of 2D organic-inorganic superlattices by LBL assembly. (a) Photographs of

thin films of PEI/MnO₂ deposited on quartz glass substrates. From a to f represent bare substrate and films with deposition cycle number of 1, 2, 5, 10, and 30. (b) UV-vis absorption spectra of multilayer films of PEI/MnO₂ prepared on a quartz glass substrate. (c) XRD pattern of as-prepared multilayer thin films of PEI/MnO₂. From a to e represent films with deposition cycle number of 1, 3, 5, 10, and 15. Reproduced with permission.⁹⁹ Copyright 2003, American Chemical Society. (d) Schematic representation for the fabrication of (CA/LDH)_n films. (e) A photograph, (f) top-view SEM image (inset: side-view SEM image), and (g) high magnification of side-view SEM image with corresponding EDX mapping analysis for the (CA/LDH)₂₀ film. Reproduced with permission.¹⁰² Copyright 2014, Wiley.

2.4 Delamination–reassembly approach

The above superlattice structures fabricated by LBL assembly processes were obtained in an ultrathin film on substrates. Bulk-scale synthesis is desirable in some practical applications. In this regard, the delamination-reassembly approach is a convenient protocol for the bulk-scale synthesis of organic-inorganic superlattices in large quantities.

Layered nanocomposites with organic polymer layers and inorganic nanosheets have been prepared by the delamination-reassembly process, including nanoclay,¹⁰⁵⁻¹⁰⁷ GO,^{108,109} layered transition metal oxides,^{110,111} transition metal dichalcogenides,¹¹²⁻¹¹⁵ and MXene.¹¹⁶⁻¹¹⁸ Yao's group synthesized interlayer-expanded MoS₂-PEO nanocomposites by a chemical delamination-reassembly method (Figure 6a). The interlayer spacing of the MoS₂-PEO nanocomposites could be controlled by changing the molar ratio between MoS₂ and PEO. By optimizing the amount of PEO during the synthesis, the MoS₂-PEO nanocomposites were achieved, accommodating one (peo₁-MoS₂) and two (peo₂-MoS₂) layers of PEO between the interlayers of MoS₂. Compared with pristine commercial MoS₂ (0.61 nm) and restacked MoS₂ without PEO (res-MoS₂) (0.62 nm), the interlayer distances of peo₁-MoS₂ and peo₂-MoS₂ were increased to 1.22, and 1.40 nm, respectively (Figure 6b).^{112,113} Well-ordered, free-standing GO-polymer nanocomposite papers were fabricated via vacuum-assisted self-assembly of mixed dispersions containing both GO nanosheets and dissolved polymers, such as poly(vinyl alcohol) (PVA) and poly(methyl methacrylate) (PMMA). Nanocomposite papers containing larger amounts of polymer exhibited larger interlayer spacings (Figure 6c). The cross-section SEM images indicated the incorporation of polymers into the structure of composites led to a thicker thickness than that of pure GO paper (Figure 6d and e).¹⁰⁸ The Ti₃C₂T_x MXene/polymer composites were also fabricated by vacuum-assisted filtration of the mixture of exfoliated Ti₃C₂T_x MXene nanosheets and either a charged PDDA or an electrically neutral PVA. The intercalation and

confinement of PVA layers between double layer $\text{Ti}_3\text{C}_2\text{T}_x$ (Figure 6f) or single-layer $\text{Ti}_3\text{C}_2\text{T}_x$ (Figure 6g) were observed in the composites with a high or low PVA content, respectively.¹¹⁷

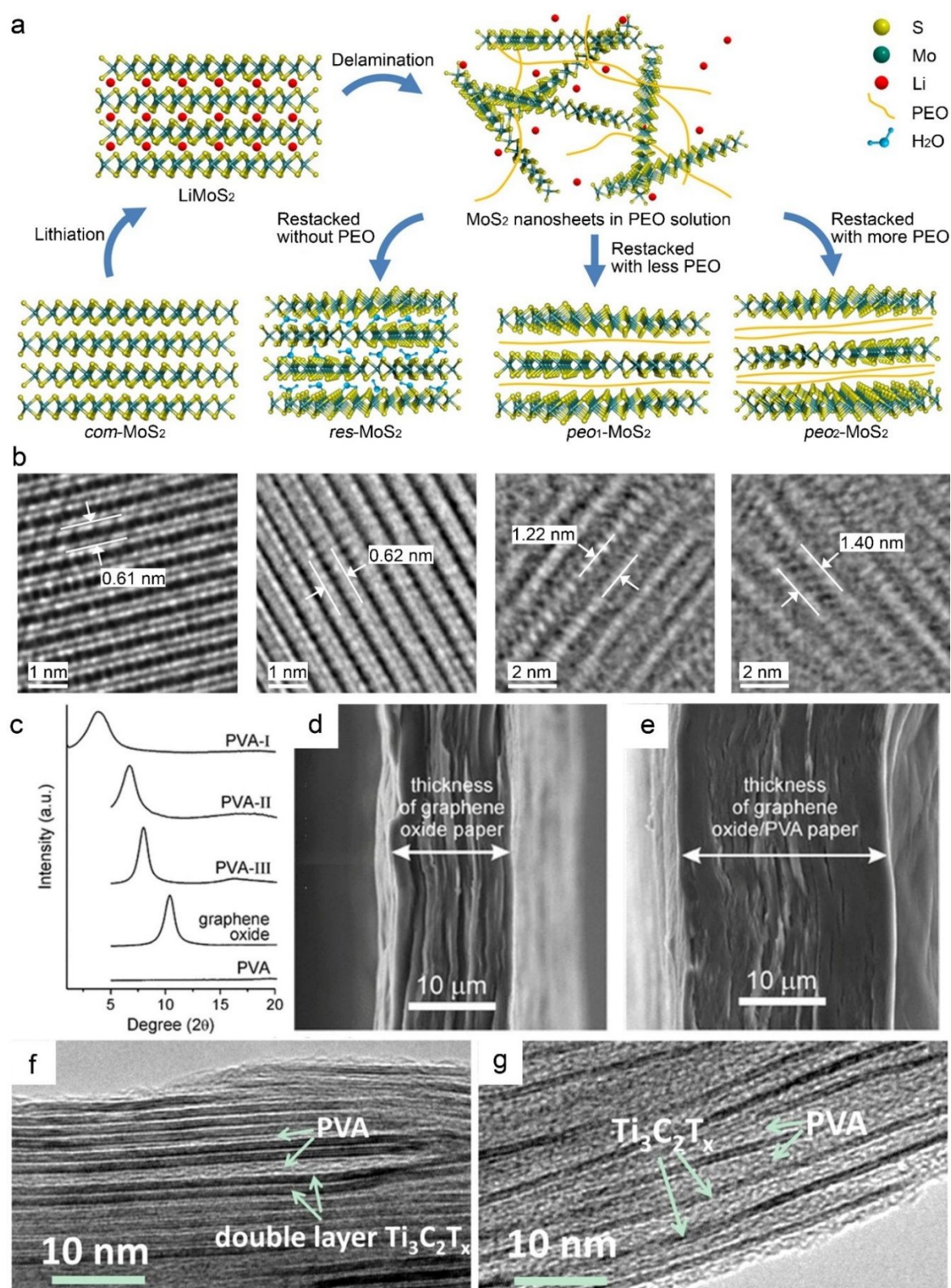


Figure 6. Fabrication of 2D organic-inorganic superlattices by delamination-reassembly approach. (a) Synthesis of interlayer expanded MoS₂-PEO composites. Commercially available com-

MoS₂ is chemically lithiated to LiMoS₂, which is then delaminated into single-layered structures in aqueous PEO solutions. Depending on the amount of PEO in the solution, three composites are obtained: simply restacked res-MoS₂ with H₂O molecules trapped within layers, peo₁-MoS₂ containing a small amount of PEO, and peo₂-MoS₂ containing a larger amount of PEO. (b) TEM images of com-MoS₂, res-MoS₂, peo₁- MoS₂, and peo₂-MoS₂. Reproduced with permission.¹¹² Copyright 2015, American Chemical Society. (c) XRD patterns of PVA, GO papers, and GO-PVA nanocomposite films. SEM images of (d) graphene oxide paper and (e) GO-PVA nanocomposite films, demonstrating increased thickness due to the intercalation of PVA. Reproduced with permission.¹⁰⁸ Copyright 2010, Wiley. Typical HRTEM images of (f) 90 wt% Ti₃C₂T_x/PVA and (g) 40 wt% Ti₃C₂T_x/PVA films showing the intercalation of PVA between Ti₃C₂T_x flakes. Reproduced with permission.¹¹⁷ Copyright 2014, National Academy of Sciences.

The 2D organic-inorganic superlattices using conjugated polymers as electrochemically active materials are more promising for energy storage applications. Boota et al. prepared a 2D organic-inorganic nanocomposite of Ti₃C₂T_x MXene combined with electrochemically active polymers, polypyrrole (PPy). Delaminated Ti₃C₂T_x nanosheets were mixed with pyrrole monomers. Then, the pyrrole monomers were polymerized between the layers of Ti₃C₂T_x nanosheets (Figure 7a), resulting in an integrated film composed of well-aligned stacked MXene sheets (Figure 7b). Hydrogen bonding between the N–H group of the pyrrole ring and terminating oxygen or fluorine present on the Ti₃C₂T_x surface may help the alignment of the polymerized PPy chains between the layers, producing a periodic pattern (Figure 7c and d).¹¹⁹ Besides, the conjugated polymers with defined properties could provide new insight into interaction mechanisms for regulation of the physical, chemical, and electrochemical properties of the resulting organic-inorganic hybrids. The same group prepared free-standing hybrid films of conjugated polymers@Ti₃C₂T_x by vacuum filtration of mixture suspensions of the conjugated polymer and Ti₃C₂T_x. Different conjugated polymers with the same conjugated backbone but different lateral chains, namely, apolar, polar, and end-charged group alkyl chains, were used to investigate the interaction mechanism with Ti₃C₂T_x nanoflakes.¹¹⁸ They found that the charged ends of the polymers were likely to play a crucial role in the intercalation process. Polar polymers with charged nitrogen-containing groups showed the strongest interaction with the Ti₃C₂T_x layers, resulting in the most obvious increase in interlayer spacing. As another electrochemically active polymer, PANI was intercalated in redox active inorganic materials, layered MnO₂ nanosheets, through a simple one-step interface reaction (Figure 7e).^{44,120} At the inorganic/organic interface, the chemical oxidation polymerization of aniline and the reduction of MnO₄²⁻ occurred simultaneously, forming a layer-by-

layer assembled PANI-MnO₂ nanolayers. The formation of PANI chains assisted the anisotropic growth of MnO₂ into 2D nanolayers. Finally, the layered PANI and MnO₂ gathered to form a mesoporous spongiform structure (Figure 7f). TEM images revealed the resulting PANI-intercalated MnO₂ composite with an expanded interlayer spacing (Figure 7g and h).

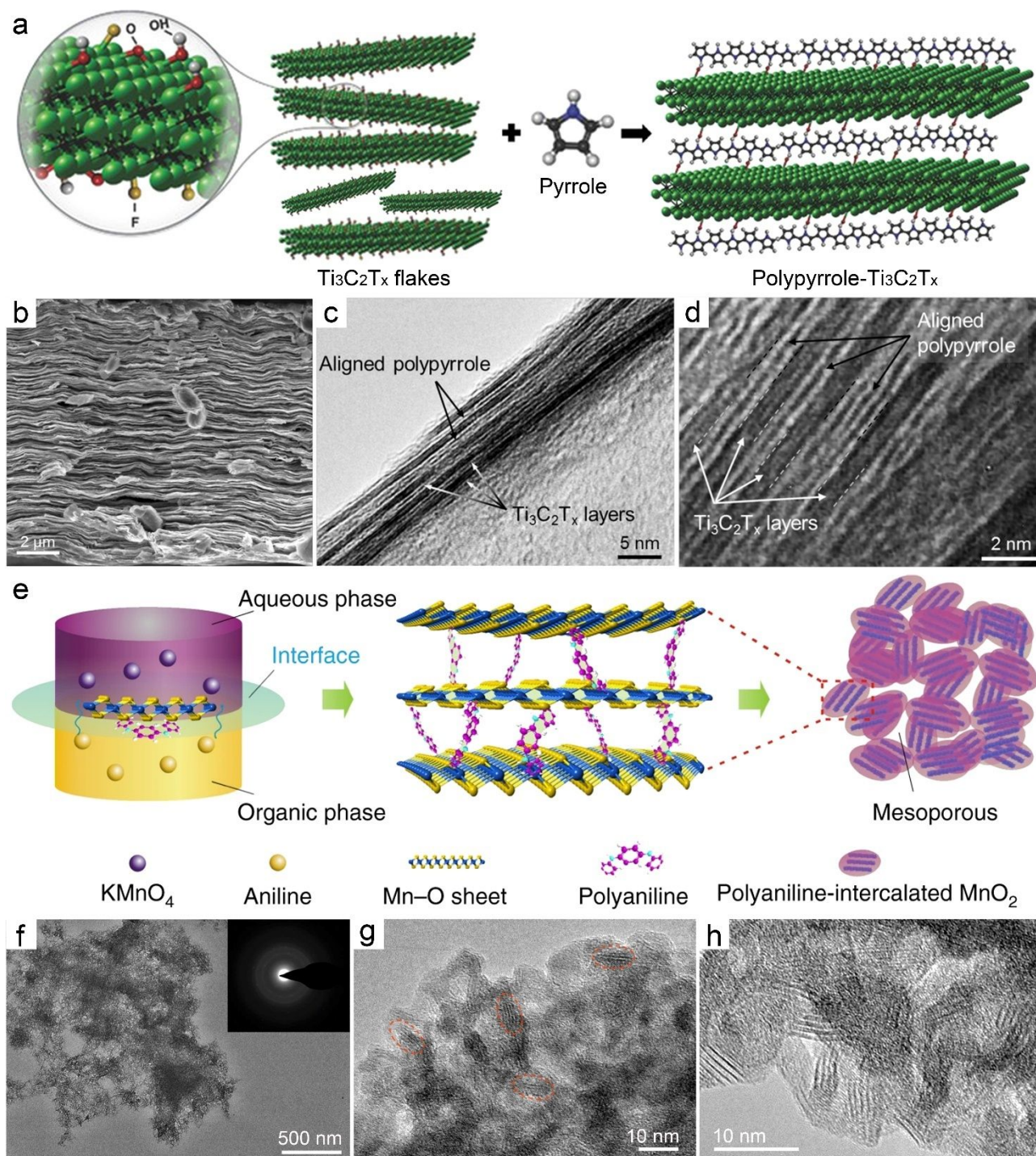


Figure 7. Fabrication of 2D organic-inorganic superlattices using conjugated polymers as electrochemically active materials. (a) Schematic illustration of pyrrole polymerization using MXene. The terminating groups on the latter contribute to the polymerization process. (b)

Cross-sectional SEM image of PPy/Ti₃C₂T_x film. (c and d) Cross-sectional TEM images of aligned polypyrrole chains between MXene sheets. Reproduced with permission.¹¹⁹ Copyright 2016, Wiley. (e) Schematic illustration of the expanded intercalated structure of polyaniline (PANI)-intercalated MnO₂ nanolayers. (f) TEM image (the inset shows the corresponding selected area electron diffraction pattern) and (g) HRTEM image of the PANI-intercalated MnO₂ nanolayers. The red dashed outlines are used to clarify the morphology profile and particle size of the MnO₂ nanolayers. (h) HR-TEM image of the PANI-intercalated MnO₂ nanolayers with heat treatment at 400 °C to remove the shield of PANI. Reproduced with permission.⁴⁴ Copyright 2018, Nature Publishing Group.

3. Energy storage applications

2D organic-inorganic superlattices are highly promising for improved performances in energy storage systems, especially the combination of electroactive inorganic nanosheets with conductive organic polymers (e.g., PANI, PPy, PEDOT) (Figure 8). The intercalation of organic polymers remarkably increases the interlayer spacing of the layered inorganic host, resulting in enhanced charge transport. Besides, the conductive polymers provide additional charge storage sites for improved capacities. More importantly, the intimate interaction between inorganic materials with organic polymers strengthens the layered structure, and thus a stable cycling performance is supposed to be achieved. Herein, we discuss the improved electrochemical performance of the 2D organic-inorganic superlattices in some energy storage systems such as supercapacitors, Li/Na/K ion batteries, and multivalent-ion batteries.

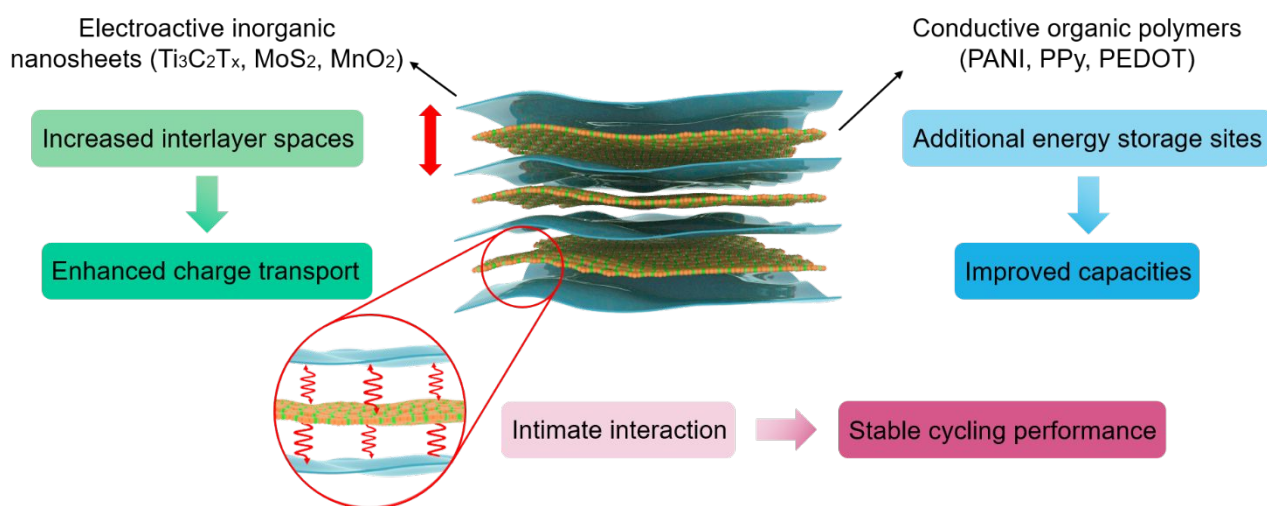


Figure 8. The advantages and synergetic effects of 2D organic-inorganic superlattices for energy storage applications. Schematic showing the advantages and possible synergetic effects in 2D organic-inorganic superlattices for energy storage application, including the increased interlayer spaces, additional energy storage sites, and intimate interaction.

3.1 Supercapacitors

Supercapacitors are promising energy storage devices due to their ultrahigh power density and excellent operating lifetime. 2D MXenes have already shown great potential in energy storage devices, especially the aqueous supercapacitors.¹²¹⁻¹²⁴ Their intrinsic metallic conductivity, in combination with atomic-scale thickness, makes them to be easily assembled into additive-free, flexible films with high electrochemical performance.¹²⁵ Furthermore, their reactive and hydrophilic surfaces render them as attractive fillers for the fabrication of MXene-polymer nanocomposites. Conductive, flexible free-standing $\text{Ti}_3\text{C}_2\text{T}_x/\text{PDDA}$ or $\text{Ti}_3\text{C}_2\text{T}_x/\text{PVA}$ composite films have been fabricated by mixing the $\text{Ti}_3\text{C}_2\text{T}_x$ flakes with PDDA or PVA, respectively.¹¹⁷ When used as electrodes for supercapacitors, the volumetric capacitance of over 300 F cm^{-3} was achieved for all $\text{Ti}_3\text{C}_2\text{T}_x$ -based films (Figure 9a), which are higher than those reported for carbon/graphene-based films.¹²⁶⁻¹²⁸ The introduction of PDDA slightly lowered the volumetric capacitance due to a lower density for the $\text{Ti}_3\text{C}_2\text{T}_x/\text{PDDA}$ film than that of pure $\text{Ti}_3\text{C}_2\text{T}_x$ film. Mixing the $\text{Ti}_3\text{C}_2\text{T}_x$ flakes with PVA-KOH gel electrolyte resulted in a dramatic increase in the volumetric capacitances, which may be due to an enlarged interlayer space (Figure 9b) and maintained high conductivities (Figure 9c). Besides, both the $\text{Ti}_3\text{C}_2\text{T}_x/\text{PDDA}$ and $\text{Ti}_3\text{C}_2\text{T}_x/\text{PVA}$ composite films showed sufficient cyclic stability (Figure 9d).

Boota et al. reported a PPy/ $\text{Ti}_3\text{C}_2\text{T}_x$ composite film as electrodes for supercapacitors. Compared with the above polymer electrolytes,¹¹⁷ the electrochemically active PPy can not only be accommodated between $\text{Ti}_3\text{C}_2\text{T}_x$ layers expanding the space for rapid charge transfer but also provide aligned paths with charge storage capability.¹¹⁹ An optimized PPy loading resulted in a high volumetric capacitance of 1000 F cm^{-3} (Figure 9e) and better rate capability than that of previously reported $\text{Ti}_3\text{C}_2\text{T}_x$ films and composite electrodes (Figure 9f). Besides, the confinement of PPy chains between $\text{Ti}_3\text{C}_2\text{T}_x$ layers may suppress the degradation of PPy. A stable cycle life up to 25000 cycles at 100 mV s^{-1} was observed for the PPy/ $\text{Ti}_3\text{C}_2\text{T}_x$ film (Figure 9g), outperforming previous PPy-containing electrodes.¹²⁹⁻¹³²

MoS_2 nanosheets have attracted tremendous attention as electrodes for supercapacitors due to their unique 2D layered structure and electronic properties.¹³³ However, their performance was still limited by the poor electrical conductivity and few accessible active sites of MoS_2 . Considerable efforts have been made to improve the conductivity and expose more active sites by intercalating conductive

materials into MoS₂ layers.¹³⁴⁻¹³⁶ Feng et al. fabricated a PEI/MoS₂ composite by direct intercalation of polymer molecules into the interlayers of MoS₂ sheets. Then, a 3D MoS₂/N-doped carbon (MoS₂/NC) composite heteroerogel was obtained through a carbonization treatment of the PEI/MoS₂ (Figure 9h).⁴⁴ The resulting heteroerogel possessed an overlapped MoS₂/C-layered heterointerface with an expanded interlayer distance of ~0.98 nm (Figure 9i). As electrode materials for supercapacitors, the MoS₂/NC exhibited high capacitances of 3550, 3150, 2900, 2670, and 2483 F g⁻¹ at current densities of 2, 4, 6, 8, and 10 A g⁻¹, respectively, demonstrating an excellent rate capability (Figure 9j). Compared with pure MoS₂ powder (Figure 9n), the 3D stably stacked and interconnected network of MoS₂/NC ensured stable ions diffusion channels and fast electron transport between MoS₂ nanosheets (Figure 9k). The expanded interlayers and intimate interfacial interactions created new pathways for efficient ion/electron transport within the MoS₂/NC heteroerogel (Figure 9l and m), which was not achieved in pure MoS₂ (Figure 9o).

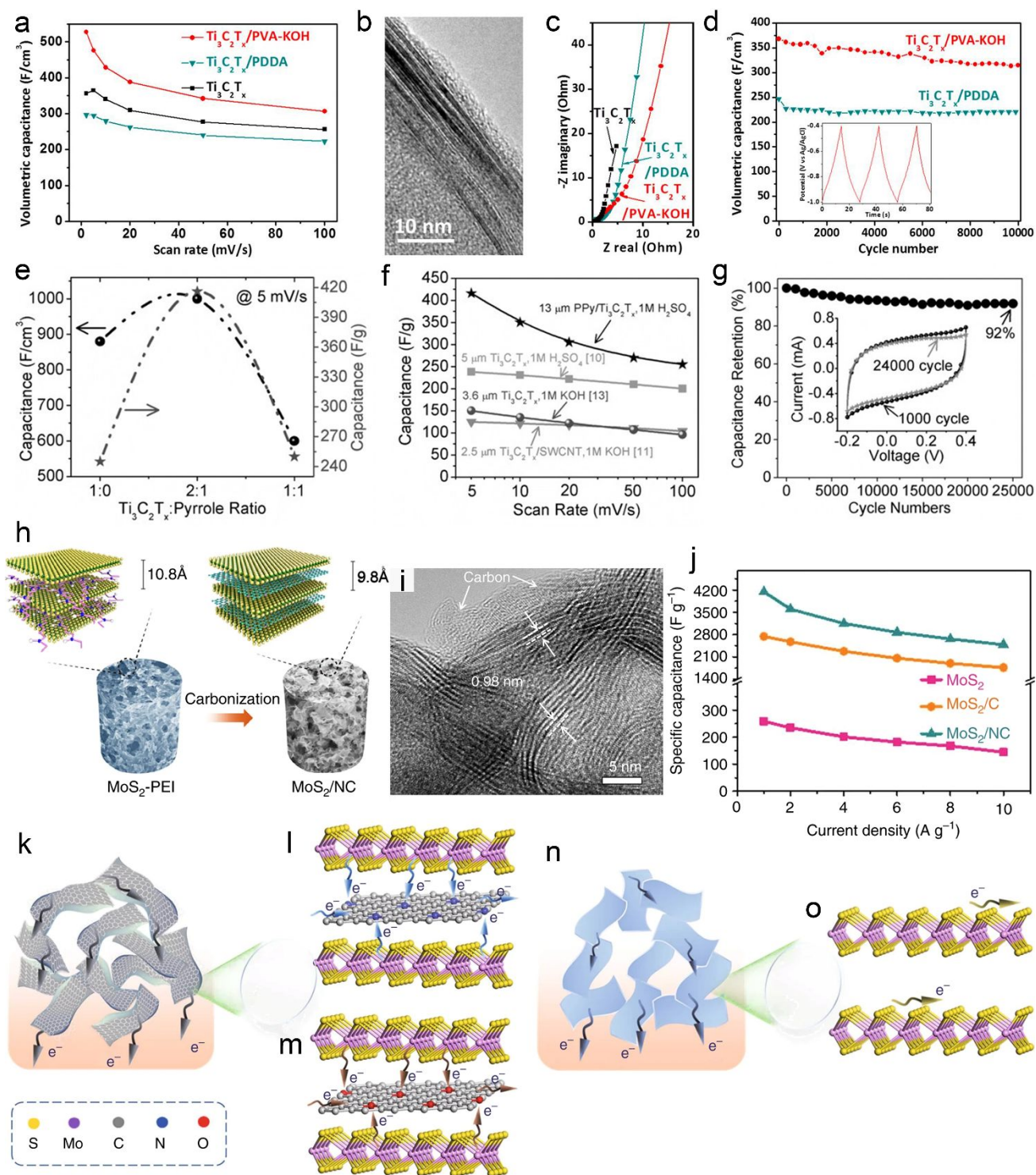


Figure 9. 2D organic-inorganic superlattices for supercapacitors. (a) Volumetric capacitances of $Ti_3C_2T_x$, $Ti_3C_2T_x/PDDA$, and $Ti_3C_2T_x/PVA-KOH$ films at different scan rates. (b) HRTEM image showing the cross-section of a $Ti_3C_2T_x/PVA-KOH$ film. (c) Nyquist plots for $Ti_3C_2T_x$, $Ti_3C_2T_x/PDDA$, and $Ti_3C_2T_x/PVA-KOH$ film electrodes. (d) Cyclic stability of $Ti_3C_2T_x/PDDA$ and $Ti_3C_2T_x/PVA-KOH$ electrodes. Reproduced with permission.¹¹⁷ Copyright 2014, National Academy of Sciences. (e) Effect of pyrrole loading on the volumetric and gravimetric capacitance of $PPy/Ti_3C_2T_x$ composites. (f) Rate performance of $PPy/Ti_3C_2T_x$ and comparisons of their capacitances with previously reported $Ti_3C_2T_x$ electrodes. (g) Cycle life performance showing high capacitance retention of the $PPy/Ti_3C_2T_x$.

film after 25000 cycles at 100 mV s^{-1} . Reproduced with permission.¹¹⁹ Copyright 2016, Wiley. (h) The schematic illustration for the synthetic procedure of the MoS₂/NC heteroerogel. (i) TEM images of the MoS₂/NC heteroerogel. (j) Rate performance of the MoS₂/NC heteroerogel. Electron transport pathways between MoS₂ nanosheets in the (k) MoS₂-based heteroerogels and (n) pure MoS₂ powder. Electron transport pathways across MoS₂ monolayers in the (l) MoS₂/NC heteroerogel and (m) MoS₂/C heteroerogel. (o) Electron transport pathways within MoS₂ monolayers in pure MoS₂ powder. Reproduced with permission.⁴⁸ Copyright 2019, Nature Publishing Group.

3.2 Li/Na/K ion batteries

Lithium-ion batteries (LIBs) with high energy density are in massive commercial adoption and manufacturing. However, Li-ion technology is plagued by high cost and limited resources. Considerable efforts have been made on alternative battery technologies such as sodium-ion batteries (SIBs) and potassium ion batteries (PIBs). Although sharing similar intercalation chemistry, the Na⁺ and K⁺ have much larger ionic radii than that of Li⁺, thus limiting the choice of electrode materials for Na and K storage. One of the most effective approaches is to increase the lattice spacing of the host materials. In this regard, the organic-inorganic superlattices with expanded interlayer spacing are promising for high-performance LIBs, SIBs, and PIBs.

Shuai et al. theoretically investigated the effect of layer spacing on Li/Na diffusion in 2H-MoS₂.¹³⁷ The diffusion path in the interlayer space started from the most stable O_h position and proceeded via the metastable T_h site before moving to the next O_h site (Figure 10a). The diffusion energy profiles for Li and Na between MoS₂ layers showed strong qualitative similarities (Figures 10b and c). The theoretical results showed that the diffusion energy barrier generally decreases as the interlayer distance increases, suggesting that layer-expanded layered materials have higher ion mobility and could achieve faster charge and discharge kinetics.^{113,138} Li et al. prepared interlayer-expanded MoS₂-PEO nanocomposites as anodes for SIBs (Figure 10d). The interlayer spacing of MoS₂ was controlled by the insertion of controlled amounts of PEO.¹¹³ The electrochemical results showed that the capacity of MoS₂ increased accordingly with the increase of interlayer distances (Figures 10e and 10f). With a 160% expansion in interlayer distance, the MoS₂-PEO exhibited a specific capacity more than twice as high as that of commercial-MoS₂.

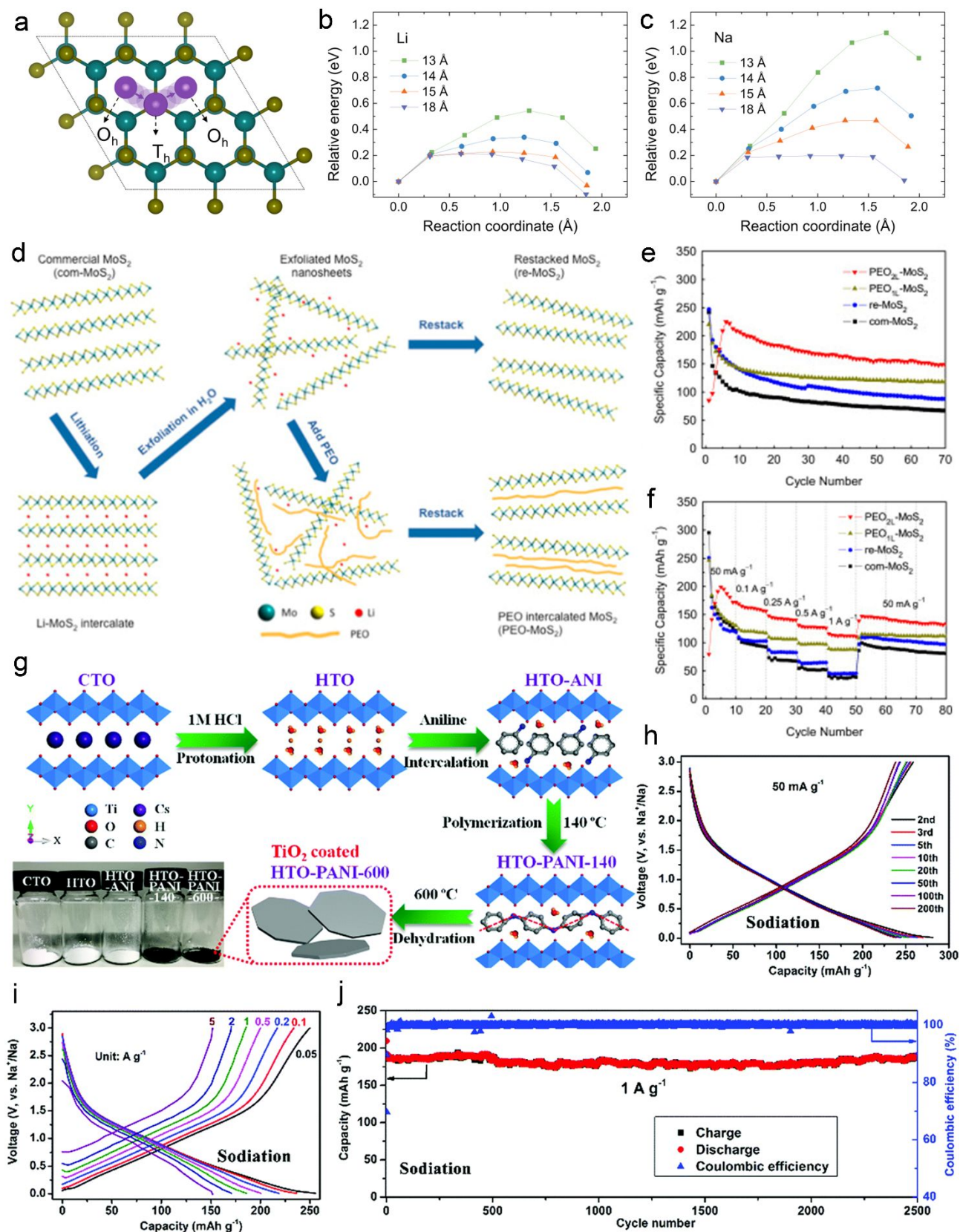


Figure 10. 2D organic-inorganic superlattices for Li/Na/K ion batteries. (a) Main diffusion path between O_h sites via a T_h site in 2H-MoS₂ layers. Relative energy along the diffusion coordinate from O_h to T_h with respect to species (b) Li and (c) Na intercalated at the most stable O_h position in 2H-MoS₂ with the indicated lattice constant c . Reproduced with permission.¹³⁷ Copyright 2016, IOP

publishing. (d) Schematic diagram of synthesis of interlayer-expanded MoS₂-PEO nanocomposites. (e) Cycling performance and (f) rate capability of MoS₂-PEO nanocomposites. Reproduced with permission.¹¹³ Copyright 2015, Elsevier. (g) Schematic illustration of the synthesis process. (h) Charge/discharge curves at 50 mA g⁻¹. (i) Discharge/charge curves at different current densities. (j) Long-life cycling performance. Reproduced with permission.⁷⁴ Copyright 2020, The Royal Society of Chemistry.

Lepidocrocite-type titanate is characterized by the orthorhombic structure composed of corrugated layers, which has shown great potential for Li/Na/K ion storage.^{139,140} Recently, Liao et al. designed a PANI intercalated protonated titanate (PANI-HTO) for SIBs and PIBs (Figure 10g).⁷² During the insertion and extraction processes of both Na and K ions, the interlayer spacing continuously changed without forming any new phase, indicating high structural reversibility. As anodes for SIBs, the PANI-HTO showed good electrochemical reversibility (Figure 10h), good rate capability (Figure 10i), and high cycling stability (Figure 10j). The high electrochemical performance of PANI-HTO should be ascribed to the beneficial effects of the intercalated polyaniline between the titanate layers. On the one hand, the intercalated PANI can play as pillars to stabilize the layered structure and enlarge the interlayer spacings for fast ion transport. On the other hand, conductive PANI can enhance the electronic conductivity of the composites. Besides, the PANI itself is a host for Na and K ion storage.^{74,141,142}

3.3 Multivalent-ion batteries

Compared with monovalent Li/Na/K ion batteries, multivalent-ion batteries are attractive for their superior theoretical volumetric energy densities because of the multi-electron transfer reactions.¹⁴³⁻¹⁴⁶ Among the multivalent-ion batteries, the aqueous zinc ion batteries (ZIBs) employing safe aqueous electrolyte and zinc metal anode have attracted increasing attention recently.¹⁴⁷⁻¹⁴⁹ However, divalent Zn²⁺ has high polarity and thus exhibit strong electrostatic/Coulombic interactions with the host lattices. This has led to a sluggish insertion and diffusion of Zn²⁺ ions into host lattices and induced a huge volume expansion of the electrode materials, resulting in a short cycle life. Vanadium-based composites have been widely investigated as host materials for ZIBs since Nazar's group explored a layered Zn_{0.25}V₂O₅ cathode for aqueous ZIBs with a high capacity and long cycling stability in 2016.¹⁵⁰ It has been demonstrated that the zinc-ion storage capacity and cycling stability of vanadium oxides cathodes can be improved through the introduction of "lubricant" into the interlayers, such as structural water, Li⁺, Na⁺, K⁺, Ca²⁺, Mg²⁺, and Zn²⁺ ions.¹⁵¹⁻¹⁵⁵ Recently, the organic molecules have

been inserted to expand the interlayer spacing and reinforce the layered structure for improved Zn storage and cycle life.⁴⁵⁻⁴⁷ For example, Xia's group employed a layered PEDOT-NH₄V₃O₈ (PEDOT-NVO) as cathodes for aqueous ZIBs.⁴⁵ Four couples of redox peaks were observed for the PEDOT-NVO cathodes, implying a multistep intercalation and deintercalation process of Zn ions. In contrast, the NVO cathodes without intercalation of PEDOT showed two redox couples (Figure 11a). The PEDOT-NVO possessed a stable layered structure with a large interlayer spacing and improved electronic conductivity, which was originated from the introduction of PEDOT. As a result, the PEDOT-NVO cathodes exhibited stable cycling stability (Figure 11b) and excellent rate capability (Figure 11c), outperforming the NVO sample. They further studied the electrochemical mechanism during the charge/discharge processes through ex-situ XRD characterizations. The layered structure of the PEDOT-NVO could be well maintained during the intercalation and deintercalation of Zn ions. Moreover, an increased *d*-spacing was accompanied by the insertion of Zn ions, whereas a decreased *d*-spacing was accompanied by the extraction of Zn ions. During the first discharge process, Zn ions were intercalated into the PEDOT-NVO. Then the Zn ions were extracted and intercalated upon the subsequent charge/discharge processes (Figure 11d).

MnO₂ has attracted much attention as cathodes for aqueous ZIBs because of its high theoretical capacity (308 mA h g⁻¹), low cost, and low toxicity.^{147,156,157} However, the development of rechargeable Zn–MnO₂ battery was severely hindered by the poor cycling stability, which was due to the serious structural transformation during cycling processes.¹⁵⁸⁻¹⁶⁰ Huang et al. reported a stable MnO₂ cathode with avoided phase transformation via intercalating the PANI polymer into layered MnO₂.⁴⁴ As a cathode for ZIBs, the PANI-MnO₂ showed two redox peaks during the cathodic sweep (Figure 11e), suggesting a two-step charge storage mechanism of H⁺ and/or Zn²⁺ insertion during the discharge process. The galvanostatic charge/discharge profile of PANI-MnO₂ showed a slope discharge profile from 1.5 to 1.33 V and a consequent discharge platform at about 1.36 V (Figure 11f). The PANI-MnO₂ cathode delivered a good rate performance with a capacity of 110 mA h g⁻¹ at a high current density of 3 A g⁻¹ (Figure 11g). At high rates, only one discharge plateau was observed, suggesting that the insertion process of H⁺ dominated the discharge process at high rates (Figure 11h). A co-insertion mechanism of H⁺ and Zn²⁺ was proposed for the PANI-MnO₂ cathode. During the first stage of discharge, H⁺ was initially inserted into PANI-MnO₂. With a sustained decrease of H⁺

concentration, the OH^- concentration is high enough to form zinc hydroxide sulfate. During the second discharge platform, the insertion of Zn^{2+} occurred, accompanying an increased amount of zinc hydroxide sulfate formed on the electrode surface (Figure 11i). Besides, the interlayer expansion strategy of organic-inorganic superlattices has also been applied in Mg storage. The expansion of interlayer distance of MoS_2 from 0.62 nm to up to 1.45 nm boosted Mg diffusivity by 2 orders of magnitude, resulting a high storage capacity and rate capability.¹¹² Although not experimentally investigated, the interlayer galleries between any adjacent organic layers and inorganic sheets can theoretically store various multivalent metal ions, including Zn^{2+} , Mg^{2+} , Ca^{2+} , and Al^{3+} ions, etc. The 2D organic-inorganic superlattices are ideal layered electrodes for multivalent-ion batteries.

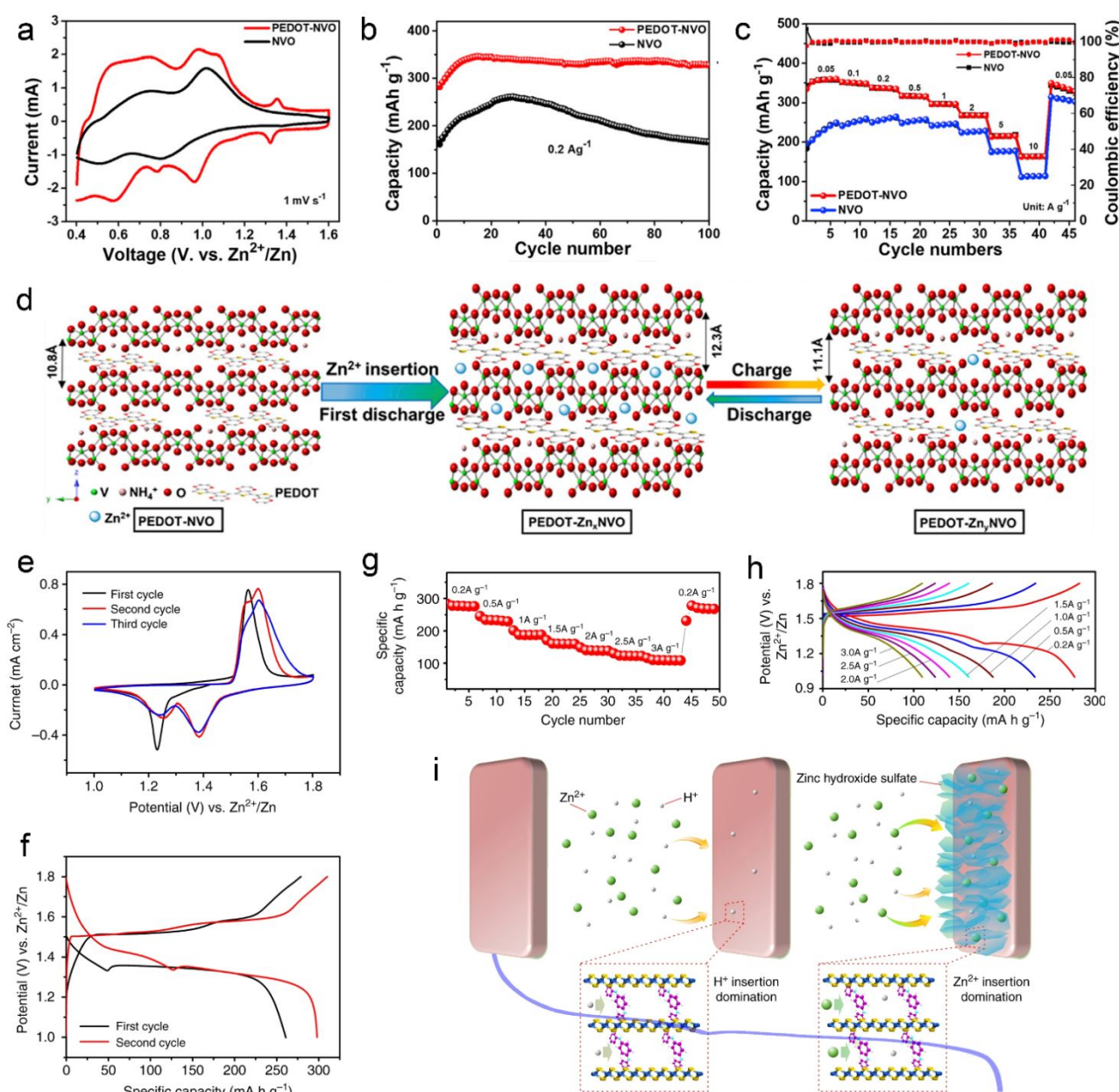


Figure 11. 2D organic-inorganic superlattices for Zn-ion batteries. (a) The second cycle of CV curves of NVO and PEDOT-NVO. (b) Cycling performance of NVO and PEDOT-NVO. (c) Rate capability of NVO and PEDOT-NVO at different current densities. (d) Schematic illustrations of Zn^{2+} intercalation into PEDOT-NVO at first discharge and subsequent extraction and intercalation upon the electrochemical charge-discharge process. Reproduced with permission.⁴⁵ Copyright 2020, Cell press. (e) Cyclic voltammetry curves of the PANI- MnO_2 . (f) Typical galvanostatic charge/discharge curves of the PANI- MnO_2 . (g and h) Rate performance and corresponding charge/discharge profiles of PANI- MnO_2 . (i) Diagram showing the sequential insertion of H^+ and Zn^{2+} . Reproduced with permission.⁴⁴ Copyright 2018, Nature Publishing Group.

4. Summary and outlook

In this review, we have summarized the recent progress on fabrication of the 2D organic-inorganic superlattices and applications of these 2D superlattices in some energy storage systems such as supercapacitors, Li/Na/K ion batteries, and multivalent ion batteries. The hybridization of 2D inorganic materials with organic materials at an atomic/molecular scale represents an ideal platform for the realization of improved or unprecedented features outperforming the individual components. The broad choice of inorganic materials and infinite variants of organic materials imply that a wide variety of 2D organic-inorganic superlattices can be produced with the desired properties. Although recent efforts have significantly advanced their fabrication, properties, and applications, the concept of 2D organic-inorganic superlattices is still at the starting stage.

Rational and scalable approaches should be explored for the controllable synthesis of 2D organic-inorganic superlattices. The nature of the intercalated polymer in the interlayer region is the decisive aspect of electrochemical performance. For example, ordered polymer chain and decreased interaction between the adjacent polymer molecules may be contributed to a high anisotropy of conductivity of the 2D organic-inorganic superlattices. One should control and optimize the molecular conformation, chain length, the oxidation state, as well as the protonation of polymers. Moreover, precise control over the atomic/molecular scale assembly of organic molecules between the inorganic layers might generate some novel properties that are not achieved from separated components. Besides, more attention should be devoted to the understanding of the intercalation mechanism of monomers, the polymerization driving force, and the interactions at organic/inorganic interfaces. A conventional blending of suspensions of organic molecules and inorganic nanosheets produced randomly mixed composites with meso- or nanoscale interactions. As we move towards the 2D superlattices, the

organic and inorganic components interact at an atomic/molecular level, boosting the importance of the interfaces. A better understanding of the nature of the interactions at organic/inorganic interfaces might lead to optimized synergetic effects for high-performance devices. In situ characterizations and, in particular, operando measurements have been widely applied in energy storage devices for investigation of energy storage mechanisms.^{161,162} These techniques are promising to probe the roles of organic/inorganic interfaces during electrochemical processes, and to study their correlation with the electrochemical performance, as well as to optimize the electrochemical performance. Molecular Dynamics (MD) simulations and Density Functional Theory (DFT) calculations have been used to investigate the electronic states at the organic-inorganic interactions.¹⁶³ Recently, machine learning has proved to have superhuman abilities in materials science.¹⁶⁴⁻¹⁶⁶ A combination of DFT calculations and machine learning techniques provides a new powerful method for tracking the interaction changes and charge transport at the organic/inorganic interfaces of 2D organic-inorganic superlattices in energy storage devices (Figure 12).

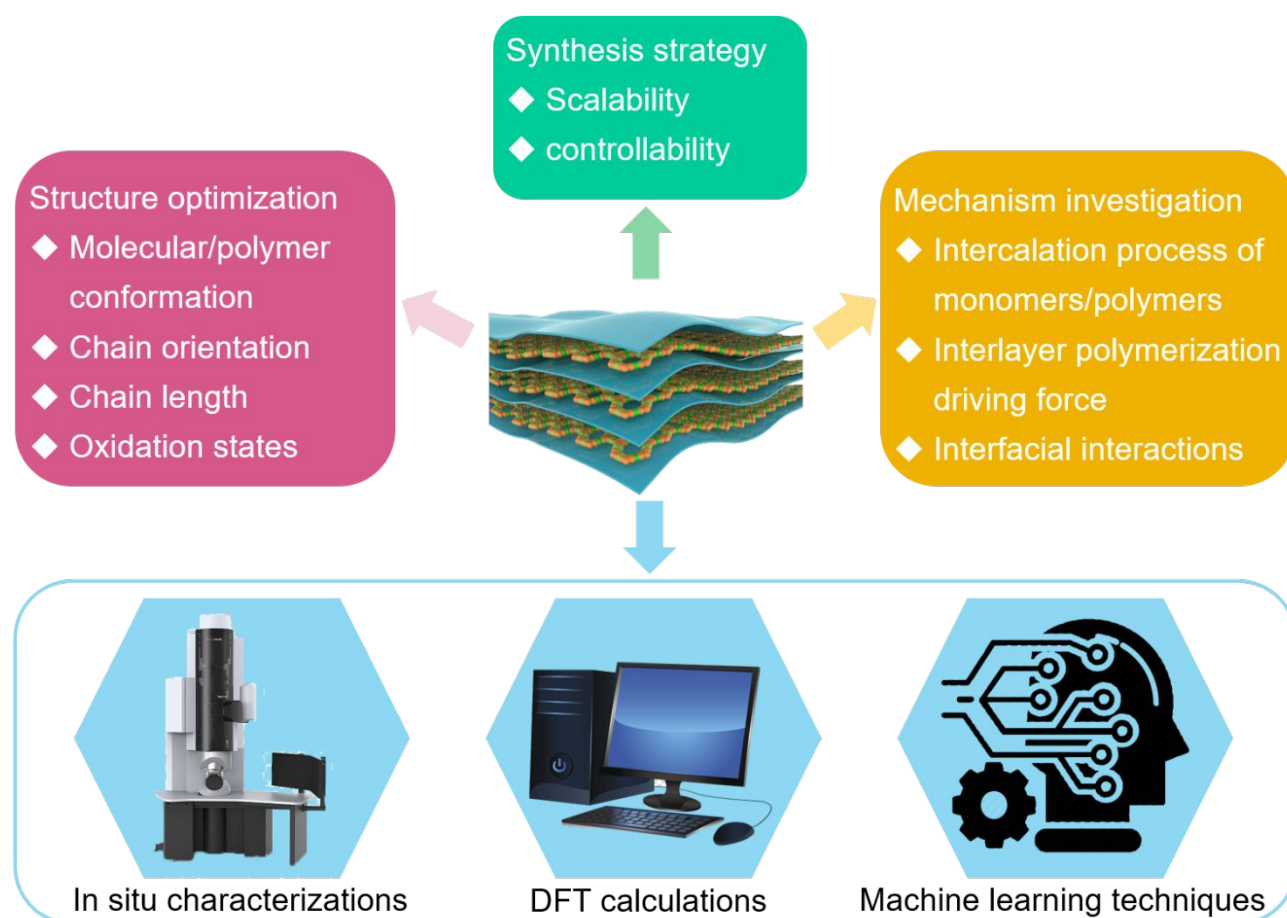


Figure 12. The challenges and direction for 2D organic-inorganic superlattices in energy storage

applications. Schematic showing the challenges of 2D organic-inorganic superlattices for energy storage application, including the synthesis strategy, structure optimization, and mechanism investigation. The future directions of in situ characterizations, DFT calculations and machine learning techniques are promising for 2D organic-inorganic superlattices in energy storage devices.

There is no doubt that the recent progress has demonstrated a bright future of 2D organic-inorganic superlattices for energy storage applications. Due to the diverse choice of inorganic and organic materials, vast new possibilities have not yet been explored. It is believed that specific superlattices by selective combinations of designed organic and inorganic materials are expected to deliver a potentially incredible performance that is not limited to the above applications but also provides a potential avenue for the current environmental and energy issues.

Acknowledgements

This work was financially supported by the Natural Science Foundation of China (No. 51772152 and No. 51902161). This work was supported in part by the WPI-MANA, Ministry of Education, Culture, Sports, Science and Technology, Japan, and CREST of the Japan Science and Technology Agency (JST). P.X. acknowledges the financial support through the startup grant from Nanjing University of Science and Technology and the Fundamental Research Funds for the Central Universities (30919011269).

References

- 1 K. S. Novoselov, A. K. Geim, S. V. Morozov, D. Jiang, Y. Zhang, S. V. Dubonos, I. V. Grigorieva and A. A. Firsov, *Science*, 2004, **306**, 666-669.
- 2 J. D. Caldwell, I. Aharonovich, G. Cassabois, J. H. Edgar, B. Gil and D. N. Basov, *Nat. Rev. Mater.*, 2019, **4**, 552-567.
- 3 S. Manzeli, D. Ovchinnikov, D. Pasquier, O. V. Yazyev and A. Kis, *Nat. Rev. Mater.*, 2017, **2**, 17033.
- 4 R. Ma and T. Sasaki, *Adv. Mater.*, 2010, **22**, 5082-5104.
- 5 R. Ma and T. Sasaki, *Acc. Chem. Res.*, 2015, **48**, 136-143.
- 6 P. Xiong, R. Ma, G. Wang and T. Sasaki, *Energy Storage Mater.*, 2019, **19**, 281-298.
- 7 B. Anasori, M. R. Lukatskaya and Y. Gogotsi, *Nat. Rev. Mater.*, 2017, **2**, 16098.
- 8 K. S. Novoselov, D. Jiang, F. Schedin, T. J. Booth, V. V. Khotkevich, S. V. Morozov and A. K. Geim, *Proc. Natl. Acad. Sci. U.S.A.*, 2005, **102**, 10451-10453.

- 9 L. Wang and T. Sasaki, *Chem. Rev.*, 2014, **114**, 9455-9486.
- 10 G. Fiori, F. Bonaccorso, G. Iannaccone, T. Palacios, D. Neumaier, A. Seabaugh, S. K. Banerjee and L. Colombo, *Nat. Nanotechnol.*, 2014, **9**, 768-779.
- 11 F. Xia, H. Wang, D. Xiao, M. Dubey and A. Ramasubramaniam, *Nat. Photonics*, 2014, **8**, 899-907.
- 12 M. Chhowalla, H. S. Shin, G. Eda, L.-J. Li, K. P. Loh and H. Zhang, *Nat. Chem.*, 2013, **5**, 263-275.
- 13 D. Akinwande, N. Petrone and J. Hone, *Nat. Commun.*, 2014, **5**, 5678.
- 14 B. Huang, G. Clark, E. Navarro-Moratalla, D. R. Klein, R. Cheng, K. L. Seyler, D. Zhong, E. Schmidgall, M. A. McGuire, D. H. Cobden, W. Yao, D. Xiao, P. Jarillo-Herrero and X. Xu, *Nature*, 2017, **546**, 270-273.
- 15 A. K. Geim and I. V. Grigorieva, *Nature*, 2013, **499**, 419-425.
- 16 R. Ma and T. Sasaki, *Ann. Rev. Mater. Res.*, 2015, **45**, 111-127.
- 17 K. S. Novoselov, A. Mishchenko, A. Carvalho and A. H. Castro Neto, *Science*, 2016, **353**, aac9439.
- 18 Y. Liu, N. O. Weiss, X. Duan, H.-C. Cheng, Y. Huang and X. Duan, *Nat. Rev. Mater.*, 2016, **1**, 16042.
- 19 P. Xiong, B. Sun, N. Sakai, R. Ma, T. Sasaki, S. Wang, J. Zhang and G. Wang, *Adv. Mater.*, 2020, **32**, 1902654.
- 20 A. Castellanos-Gomez, M. Buscema, R. Molenaar, V. Singh, L. Janssen, H. S. J. van der Zant and G. A. Steele, *2D Mater.*, 2014, **1**, 011002.
- 21 L. Britnell, R. V. Gorbachev, R. Jalil, B. D. Belle, F. Schedin, A. Mishchenko, T. Georgiou, M. I. Katsnelson, L. Eaves, S. V. Morozov, N. M. R. Peres, J. Leist, A. K. Geim, K. S. Novoselov and L. A. Ponomarenko, *Science*, 2012, **335**, 947-950.
- 22 L. Britnell, R. V. Gorbachev, A. K. Geim, L. A. Ponomarenko, A. Mishchenko, M. T. Greenaway, T. M. Fromhold, K. S. Novoselov and L. Eaves, *Nat. Commun.*, 2013, **4**, 1794.
- 23 C.-H. Lee, G.-H. Lee, A. M. van der Zande, W. Chen, Y. Li, M. Han, X. Cui, G. Arefe, C. Nuckolls, T. F. Heinz, J. Guo, J. Hone and P. Kim, *Nat. Nanotechnol.*, 2014, **9**, 676-681.
- 24 F. Withers, O. Del Pozo-Zamudio, A. Mishchenko, A. P. Rooney, A. Gholinia, K. Watanabe, T. Taniguchi, S. J. Haigh, A. K. Geim, A. I. Tartakovskii and K. S. Novoselov, *Nat. Mater.*, 2015,

- 14**, 301-306.
- 25 E. Pomerantseva and Y. Gogotsi, *Nat. Energy*, 2017, **2**, 17089.
- 26 D. Deng, K. S. Novoselov, Q. Fu, N. Zheng, Z. Tian and X. Bao, *Nat. Nanotechnol.*, 2016, **11**, 218-230.
- 27 A. Narita, X.-Y. Wang, X. Feng and K. Müllen, *Chem. Soc. Rev.*, 2015, **44**, 6616-6643.
- 28 Y. Liu, A. Narita, J. Teyssandier, M. Wagner, S. De Feyter, X. Feng and K. Müllen, *J. Am. Chem. Soc.*, 2016, **138**, 15539-15542.
- 29 M. Gobbi, E. Orgiu and P. Samorì, *Adv. Mater.*, 2018, **30**, 1706103.
- 30 Y. Zhong, B. Cheng, C. Park, A. Ray, S. Brown, F. Mujid, J.-U. Lee, H. Zhou, J. Suh, K.-H. Lee, A. J. Mannix, K. Kang, S. J. Sibener, D. A. Muller and J. Park, *Science*, 2019, **366**, 1379-1384.
- 31 Y. Huang, J. Liang, C. Wang, S. Yin, W. Fu, H. Zhu and C. Wan, *Chem. Soc. Rev.*, 2020, **49**, 6866-6883.
- 32 M. Servalli and A. D. Schlüter, *Ann. Rev. Mater. Res.*, 2017, **47**, 361-389.
- 33 P. Payamyar, B. T. King, H. C. Öttinger and A. D. Schlüter, *Chem. Commun.*, 2016, **52**, 18-34.
- 34 D. F. Perepichka and F. Rosei, *Science*, 2009, **323**, 216-217.
- 35 G. Franc and A. Gourdon, *Phys. Chem. Chem. Phys.*, 2011, **13**, 14283-14292.
- 36 H. Furukawa, K. E. Cordova, M. O’Keeffe and O. M. Yaghi, *Science*, 2013, **341**, 1230444.
- 37 P. J. Waller, F. Gándara and O. M. Yaghi, *Acc. Chem. Res.*, 2015, **48**, 3053-3063.
- 38 P. Gomez-Romero, *Adv. Mater.*, 2001, **13**, 163-174.
- 39 W. Wu, Y. Liu and D. Zhu, *Chem. Soc. Rev.*, 2010, **39**, 1489-1502.
- 40 P. M. Beaujuge and J. M. J. Fréchet, *J. Am. Chem. Soc.*, 2011, **133**, 20009-20029.
- 41 E. Ruiz-Hitzky, *Adv. Mater.*, 1993, **5**, 334-340.
- 42 P. Xiong, J. Zhu and X. Wang, *J. Power Sources*, 2015, **294**, 31-50.
- 43 P. Xiong, J. Zhu, L. Zhang, X. Wang, *Nanoscale Horiz.*, 2016, **1**, 340-374.
- 44 J. Huang, Z. Wang, M. Hou, X. Dong, Y. Liu, Y. Wang and Y. Xia, *Nat. Commun.*, 2018, **9**, 2906.
- 45 D. Bin, W. Huo, Y. Yuan, J. Huang, Y. Liu, Y. Zhang, F. Dong, Y. Wang and Y. Xia, *Chem*, 2020, **6**, 968-984.
- 46 Z. Yao, Q. Wu, K. Chen, J. Liu and C. Li, *Energy Environ. Sci.*, 2020, **13**, 3149-3163.
- 47 S. Chen, K. Li, K. S. Hui and J. Zhang, *Adv. Funct. Mater.*, 2020, 2003890.

- 48 N. Feng, R. Meng, L. Zu, Y. Feng, C. Peng, J. Huang, G. Liu, B. Chen and J. Yang, *Nat. Commun.*, 2019, **10**, 1372.
- 49 K. Chang, W. Chen, L. Ma, H. Li, H. Li, F. Huang, Z. Xu, Q. Zhang and J.-Y. Lee, *J. Mater. Chem.*, 2011, **21**, 6251-6257.
- 50 M.-R. Gao, M. K. Y. Chan and Y. Sun, *Nat. Commun.*, 2015, **6**, 7493.
- 51 H. Jiang, D. Ren, H. Wang, Y. Hu, S. Guo, H. Yuan, P. Hu, L. Zhang and C. Li, *Adv. Mater.*, 2015, **27**, 3687-3695.
- 52 N. Liu, Y. Guo, X. Yang, H. Lin, L. Yang, Z. Shi, Z. Zhong, S. Wang, Y. Tang and Q. Gao, *ACS Appl. Mater. Interfaces*, 2015, **7**, 23741-23749.
- 53 Q. Liu, X. Li, Q. He, A. Khalil, D. Liu, T. Xiang, X. Wu and L. Song, *Small*, 2015, **11**, 5556-5564.
- 54 X. Wang, Z. Guan, Y. Li, Z. Wang and L. Chen, *Nanoscale*, 2015, **7**, 637-641.
- 55 J. Xie, J. Zhang, S. Li, F. Grote, X. Zhang, H. Zhang, R. Wang, Y. Lei, B. Pan and Y. Xie, *J. Am. Chem. Soc.*, 2013, **135**, 17881-17888.
- 56 X. Zhao, C. Hu and M. Cao, *Chem. Asian J.*, 2013, **8**, 2701-2707.
- 57 L. Hu, Y. Ren, H. Yang and Q. Xu, *ACS Appl. Mater. Interfaces*, 2014, **6**, 14644-14652.
- 58 Y. Matsuo, S. Higashika, K. Kimura, Y. Miyamoto, T. Fukutsuka and Y. Sugie, *J. Mater. Chem.*, 2002, **12**, 1592-1596.
- 59 X. Zhang, L. Ji, S. Zhang and W. Yang, *J. Power Sources*, 2007, **173**, 1017-1023.
- 60 M. G. Kanatzidis, C.-G. Wu, H. O. Marcy, D. C. DeGroot, C. R. Kannewurf, A. Kostikas and V. Papaefthymiou, *Adv. Mater.*, 1990, **2**, 364-366.
- 61 M. G. Kanatzidis, C. G. Wu, H. O. Marcy and C. R. Kannewurf, *J. Am. Chem. Soc.*, 1989, **111**, 4139-4141.
- 62 C. G. Wu, D. C. DeGroot, H. O. Marcy, J. L. Schindler, C. R. Kannewurf, T. Bakas, V. Papaefthymiou, W. Hirpo and J. P. Yesinowski, *J. Am. Chem. Soc.*, 1995, **117**, 9229-9242.
- 63 C. G. Wu, D. C. DeGroot, H. O. Marcy, J. L. Schindler, C. R. Kannewurf, Y. J. Liu, W. Hirpo and M. G. Kanatzidis, *Chem. Mater.*, 1996, **8**, 1992-2004.
- 64 S. Pang, G. Li and Z. Zhang, *Macromol. Rapid Commun.*, 2005, **26**, 1262-1265.
- 65 Y. Chen, G. Yang, Z. Zhang, X. Yang, W. Hou and J.-J. Zhu, *Nanoscale*, 2010, **2**, 2131-2138.

- 66 I. Boyano, M. Bengoechea, I. de Meatza, O. Miguel, I. Cantero, E. Ochoteco, J. Rodríguez, M. Lira-Cantú and P. Gómez-Romero, *J. Power Sources*, 2007, **166**, 471-477.
- 67 C. X. Guo, K. Sun, J. Ouyang and X. Lu, *Chem. Mater.*, 2015, **27**, 5813-5819.
- 68 A. V. Murugan, B. B. Kale, C.-W. Kwon, G. Campet and K. Vijayamohanan, *J. Mater. Chem.*, 2001, **11**, 2470-2475.
- 69 S. H. Lee, C. Park, J. W. Park, S. J. Kim, S. S. Im and H. Ahn, *J. Power Sources*, 2019, **414**, 460-469.
- 70 K. J. Chao, T. C. Chang and S. Y. Ho, *J. Mater. Chem.*, 1993, **3**, 427-428.
- 71 L. Wang, P. Brazis, M. Rocci, C. R. Kannewurf and M. G. Kanatzidis, *Chem. Mater.*, 1998, **10**, 3298-3300.
- 72 P. Xiao, M. Xiao, P. Liu and K. Gong, *Carbon*, 2000, **38**, 626-628.
- 73 G. Yang, W. Hou, X. Feng, L. Xu, Y. Liu, G. Wang and W. Ding, *Adv. Funct. Mater.*, 2007, **17**, 401-412.
- 74 J. Liao, Q. Hu, J. Mu, F. Chen, X. He, F. Chen, Z. Wen and C. Chen, *Chem. Commun.*, 2020, **56**, 8392-8395.
- 75 C. Wan, X. Gu, F. Dang, T. Itoh, Y. Wang, H. Sasaki, M. Kondo, K. Koga, K. Yabuki, G. J. Snyder, R. Yang and K. Koumoto, *Nat. Mater.*, 2015, **14**, 622-627.
- 76 C. Wan, R. Tian, M. Kondou, R. Yang, P. Zong and K. Koumoto, *Nat. Commun.*, 2017, **8**, 1024.
- 77 C. Wan, Y. Kodama, M. Kondo, R. Sasai, X. Qian, X. Gu, K. Koga, K. Yabuki, R. Yang and K. Koumoto, *Nano Lett.*, 2015, **15**, 6302-6308.
- 78 C. Wang, Q. He, U. Halim, Y. Liu, E. Zhu, Z. Lin, H. Xiao, X. Duan, Z. Feng, R. Cheng, N. O. Weiss, G. Ye, Y.-C. Huang, H. Wu, H.-C. Cheng, I. Shakir, L. Liao, X. Chen, W. A. Goddard Iii, Y. Huang and X. Duan, *Nature*, 2018, **555**, 231-236.
- 79 G. Decher, *Science*, 1997, **277**, 1232-1237.
- 80 J. H. Fendler, *Chem. Mater.*, 1996, **8**, 1616-1624.
- 81 T. Cassagneau, T. E. Mallouk and J. H. Fendler, *J. Am. Chem. Soc.*, 1998, **120**, 7848-7859.
- 82 F. Caruso and H. Möhwald, *J. Am. Chem. Soc.*, 1999, **121**, 6039-6046.
- 83 Z. Tang, N. A. Kotov, S. Magonov and B. Ozturk, *Nat. Mater.*, 2003, **2**, 413-418.
- 84 P. T. Hammond, *Adv. Mater.*, 2004, **16**, 1271-1293.

- 85 C. Jiang and V. V. Tsukruk, *Adv. Mater.*, 2006, **18**, 829-840.
- 86 Z. Tang, Y. Wang, P. Podsiadlo and N. A. Kotov, *Adv. Mater.*, 2006, **18**, 3203-3224.
- 87 P. Podsiadlo, A. K. Kaushik, E. M. Arruda, A. M. Waas, B. S. Shim, J. Xu, H. Nandivada, B. G. Pumplun, J. Lahann, A. Ramamoorthy and N. A. Kotov, *Science*, 2007, **318**, 80-83.
- 88 E. R. Kleinfeld and G. S. Ferguson, *Science*, 1994, **265**, 370-373.
- 89 S. W. Keller, H.-N. Kim and T. E. Mallouk, *J. Am. Chem. Soc.*, 1994, **116**, 8817-8818.
- 90 C. Kranz, H. E. Gaub and W. Schuhmann, *Adv. Mater.*, 1996, **8**, 634-637.
- 91 M. Fang, D. M. Kaschak, A. C. Sutorik and T. E. Mallouk, *J. Am. Chem. Soc.*, 1997, **119**, 12184-12191.
- 92 N. A. Kotov, S. Magonov and E. Tropsha, *Chem. Mater.*, 1998, **10**, 886-895.
- 93 T. Sasaki, Y. Ebina, M. Watanabe and G. Decher, *Chem. Commun.*, 2000, 2163-2164.
- 94 T. Sasaki, Y. Ebina, T. Tanaka, M. Harada, M. Watanabe and G. Decher, *Chem. Mater.*, 2001, **13**, 4661-4667.
- 95 M. Ferreira, V. Zucolotto, F. Huguenin, R. M. Torresi and O. N. Oliveira, *J. Nanosci. Nanotechnol.*, 2002, **2**, 29-32.
- 96 R. E. Schaak and T. E. Mallouk, *Chem. Mater.*, 2002, **14**, 1455-1471.
- 97 T. Sasaki, Y. Ebina, K. Fukuda, T. Tanaka, M. Harada and M. Watanabe, *Chem. Mater.*, 2002, **14**, 3524-3530.
- 98 M. Ferreira, F. Huguenin, V. Zucolotto, J. E. Pereira da Silva, S. I. Córdoba de Torresi, M. L. A. Temperini, R. M. Torresi and O. N. Oliveira, *J. Phys. Chem. B*, 2003, **107**, 8351-8354.
- 99 L. Wang, Y. Omomo, N. Sakai, K. Fukuda, I. Nakai, Y. Ebina, K. Takada, M. Watanabe and T. Sasaki, *Chem. Mater.*, 2003, **15**, 2873-2878.
- 100 J. Huang, R. Ma, Y. Ebina, K. Fukuda, K. Takada and T. Sasaki, *Chem. Mater.*, 2010, **22**, 2582-2587.
- 101 H.-B. Yao, H.-Y. Fang, Z.-H. Tan, L.-H. Wu and S.-H. Yu, *Angew. Chem. Int. Ed.*, 2010, **49**, 2140-2145.
- 102 Y. Dou, S. Xu, X. Liu, J. Han, H. Yan, M. Wei, D. G. Evans and X. Duan, *Adv. Funct. Mater.*, 2014, **24**, 514-521.
- 103 Z. Liu, R. Ma, M. Osada, N. Iyi, Y. Ebina, K. Takada and T. Sasaki, *J. Am. Chem. Soc.*, 2006,

- 128**, 4872-4880.
- 104 L. Li, R. Ma, N. Iyi, Y. Ebina, K. Takada and T. Sasaki, *Chem. Commun.*, 2006, 3125-3127.
- 105 A. Walther, I. Bjurhager, J.-M. Malho, J. Pere, J. Ruokolainen, L. A. Berglund and O. Ikkala, *Nano Lett.*, 2010, **10**, 2742-2748.
- 106 A. Walther, I. Bjurhager, J.-M. Malho, J. Ruokolainen, L. Berglund and O. Ikkala, *Angew. Chem. Int. Ed.*, 2010, **49**, 6448-6453.
- 107 J. Wang, Q. Cheng, L. Lin and L. Jiang, *ACS Nano*, 2014, **8**, 2739-2745.
- 108 K. W. Putz, O. C. Compton, M. J. Palmeri, S. T. Nguyen and L. C. Brinson, *Adv. Funct. Mater.*, 2010, **20**, 3322-3329.
- 109 Y. Tian, Y. Cao, Y. Wang, W. Yang and J. Feng, *Adv. Mater.*, 2013, **25**, 2980-2983.
- 110 Z.-H. Liu, X. Yang, Y. Makita and K. Ooi, *Chem. Mater.*, 2002, **14**, 4800-4806.
- 111 N. Sukpirom and M. M. Lerner, *Chem. Mater.*, 2001, **13**, 2179-2185.
- 112 Y. Liang, H. D. Yoo, Y. Li, J. Shuai, H. A. Calderon, F. C. Robles Hernandez, L. C. Grabow and Y. Yao, *Nano Lett.*, 2015, **15**, 2194-2202.
- 113 Y. Li, Y. Liang, F. C. Robles Hernandez, H. Deog Yoo, Q. An and Y. Yao, *Nano Energy*, 2015, **15**, 453-461.
- 114 J. P. Lemmon and M. M. Lerner, *Chem. Mater.*, 1994, **6**, 207-210.
- 115 X. Qian, K. Xie, S. Guo, Q. Liang, S. Zhang, Z. Xiong, H. Zhan, C. Liu, X. Yang, J. Zhu and D. Li, *Chem. Commun.*, 2020, **56**, 7005-7008.
- 116 X. Zhang, J. Xu, H. Wang, J. Zhang, H. Yan, B. Pan, J. Zhou and Y. Xie, *Angew. Chem. Int. Ed.*, 2013, **52**, 4361-4365.
- 117 Z. Ling, C. E. Ren, M.-Q. Zhao, J. Yang, J. M. Giammarco, J. Qiu, M. W. Barsoum and Y. Gogotsi, *Proc. Natl. Acad. Sci. U.S.A.*, 2014, **111**, 16676-16681.
- 118 M. Boota, M. Pasini, F. Galeotti, W. Porzio, M.-Q. Zhao, J. Halim and Y. Gogotsi, *Chem. Mater.*, 2017, **29**, 2731-2738.
- 119 M. Boota, B. Anasori, C. Voigt, M.-Q. Zhao, M. W. Barsoum and Y. Gogotsi, *Adv. Mater.*, 2016, **28**, 1517-1522.
- 120 Y.-G. Wang, W. Wu, L. Cheng, P. He, C.-X. Wang and Y.-Y. Xia, *Adv. Mater.*, 2008, **20**, 2166-2170.

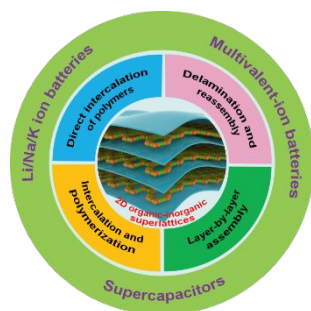
- 121 M. Naguib, J. Halim, J. Lu, K. M. Cook, L. Hultman, Y. Gogotsi and M. W. Barsoum, *J. Am. Chem. Soc.*, 2013, **135**, 15966-15969.
- 122 X. Liang, A. Garsuch and L. F. Nazar, *Angew. Chem. Int. Ed.*, 2015, **54**, 3907-3911.
- 123 X. Wang, S. Kajiyama, H. Iinuma, E. Hosono, S. Oro, I. Moriguchi, M. Okubo and A. Yamada, *Nat. Commun.*, 2015, **6**, 6544.
- 124 M. Ghidui, M. R. Lukatskaya, M.-Q. Zhao, Y. Gogotsi and M. W. Barsoum, *Nature*, 2014, **516**, 78-81.
- 125 M. R. Lukatskaya, O. Mashtalir, C. E. Ren, Y. Dall'Agnese, P. Rozier, P. L. Taberna, M. Naguib, P. Simon, M. W. Barsoum and Y. Gogotsi, *Science*, 2013, **341**, 1502-1505.
- 126 Y. Zhu, S. Murali, M. D. Stoller, K. J. Ganesh, W. Cai, P. J. Ferreira, A. Pirkle, R. M. Wallace, K. A. Cychosz, M. Thommes, D. Su, E. A. Stach and R. S. Ruoff, *Science*, 2011, **332**, 1537-1541.
- 127 M. Heon, S. Lofland, J. Applegate, R. Nolte, E. Cortes, J. D. Hettinger, P.-L. Taberna, P. Simon, P. Huang, M. Brunet and Y. Gogotsi, *Energy Environ. Sci.*, 2011, **4**, 135-138.
- 128 X. Yang, C. Cheng, Y. Wang, L. Qiu and D. Li, *Science*, 2013, **341**, 534-537.
- 129 T. Liu, L. Finn, M. Yu, H. Wang, T. Zhai, X. Lu, Y. Tong and Y. Li, *Nano Lett.*, 2014, **14**, 2522-2527.
- 130 H. Tang, J. Wang, H. Yin, H. Zhao, D. Wang and Z. Tang, *Adv. Mater.*, 2015, **27**, 1117-1123.
- 131 S. Biswas and L. T. Drzal, *Chem. Mater.*, 2010, **22**, 5667-5671.
- 132 M. Hughes, G. Z. Chen, M. S. P. Shaffer, D. J. Fray and A. H. Windle, *Chem. Mater.*, 2002, **14**, 1610-1613.
- 133 M. Acerce, D. Voiry and M. Chhowalla, *Nat. Nanotechnol.*, 2015, **10**, 313-318.
- 134 D. Kong, H. He, Q. Song, B. Wang, W. Lv, Q.-H. Yang and L. Zhi, *Energy Environ. Sci.*, 2014, **7**, 3320-3325.
- 135 C. Zhao, X. Wang, J. Kong, J. M. Ang, P. S. Lee, Z. Liu and X. Lu, *ACS Appl. Mater. Interfaces*, 2016, **8**, 2372-2379.
- 136 P. Xiong, R. Ma, N. Sakai, L. Nurdiwijayanto and T. Sasaki, *ACS Energy Lett.*, 2018, **3**, 997-1005.
- 137 J. Shuai, H. D. Yoo, Y. Liang, Y. Li, Y. Yao and L. C. Grabow, *Mater. Res. Express*, 2016, **3**, 064001.
- 138 P. Xiong, R. Ma, N. Sakai, X. Bai, S. Li and T. Sasaki, *ACS Appl. Mater. Interfaces*, 2017, **9**,

6282-6291.

- 139 P. Xiong, X. Zhang, F. Zhang, D. Yi, J. Zhang, B. Sun, H. Tian, D. Shanmukaraj, T. Rojo, M. Armand, R. Ma, T. Sasaki and G. Wang, *ACS Nano*, 2018, **12**, 12337-12346.
- 140 J. Yang, X. Xiao, W. Gong, L. Zhao, G. Li, K. Jiang, R. Ma, M. H. Rummeli, F. Li, T. Sasaki and F. Geng, *Angew. Chem. Int. Ed.*, 2019, **58**, 8740-8745.
- 141 Q. Zhou, L. Liu, Z. Huang, L. Yi, X. Wang and G. Cao, *J. Mater. Chem. A*, 2016, **4**, 5505-5516.
- 142 H. Gao, L. Xue, S. Xin and J. B. Goodenough, *Angew. Chem. Int. Ed.*, 2018, **57**, 5449-5453.
- 143 M. Li, J. Lu, X. Ji, Y. Li, Y. Shao, Z. Chen, C. Zhong and K. Amine, *Nat. Rev. Mater.*, 2020, **5**, 276-294.
- 144 A. Ponrouch, J. Bitenc, R. Dominko, N. Lindahl, P. Johansson and M. R. Palacin, *Energy Storage Mater.*, 2019, **20**, 253-262.
- 145 P. Xiong, F. Zhang, X. Zhang, S. Wang, H. Liu, B. Sun, J. Zhang, Y. Sun, R. Ma, Y. Bando, C. Zhou, Z. Liu, T. Sasaki and G. Wang, *Nat. Commun.*, 2020, **11**, 3297.
- 146 Y. Liang, H. Dong, D. Aurbach and Y. Yao, *Nat. Energy*, 2020, **5**, 646-656.
- 147 N. Zhang, F. Cheng, J. Liu, L. Wang, X. Long, X. Liu, F. Li and J. Chen, *Nat. Commun.*, 2017, **8**, 405.
- 148 G. Fang, J. Zhou, A. Pan and S. Liang, *ACS Energy Lett.*, 2018, **3**, 2480-2501.
- 149 M. Song, H. Tan, D. Chao and H. J. Fan, *Adv. Funct. Mater.*, 2018, **28**, 1802564.
- 150 D. Kundu, B. D. Adams, V. Duffort, S. H. Vajargah and L. F. Nazar, *Nat. Energy*, 2016, **1**, 16119.
- 151 M. Yan, P. He, Y. Chen, S. Wang, Q. Wei, K. Zhao, X. Xu, Q. An, Y. Shuang, Y. Shao, K. T. Mueller, L. Mai, J. Liu and J. Yang, *Adv. Mater.*, 2018, **30**, 1703725.
- 152 Y. Yang, Y. Tang, G. Fang, L. Shan, J. Guo, W. Zhang, C. Wang, L. Wang, J. Zhou and S. Liang, *Energy Environ. Sci.*, 2018, **11**, 3157-3162.
- 153 P. He, G. Zhang, X. Liao, M. Yan, X. Xu, Q. An, J. Liu and L. Mai, *Adv. Energy Mater.*, 2018, **8**, 1702463.
- 154 C. Xia, J. Guo, P. Li, X. Zhang and H. N. Alshareef, *Angew. Chem. Int. Ed.*, 2018, **57**, 3943-3948.
- 155 F. Ming, H. Liang, Y. Lei, S. Kandambeth, M. Eddaoudi and H. N. Alshareef, *ACS Energy Lett.*, 2018, **3**, 2602-2609.
- 156 H. Pan, Y. Shao, P. Yan, Y. Cheng, K. S. Han, Z. Nie, C. Wang, J. Yang, X. Li, P. Bhattacharya,

- K. T. Mueller and J. Liu, *Nat. Energy*, 2016, **1**, 16039.
- 157 W. Sun, F. Wang, S. Hou, C. Yang, X. Fan, Z. Ma, T. Gao, F. Han, R. Hu, M. Zhu and C. Wang, *J. Am. Chem. Soc.*, 2017, **139**, 9775-9778.
- 158 N. D. Ingale, J. W. Gallaway, M. Nyce, A. Couzis and S. Banerjee, *J. Power Sources*, 2015, **276**, 7-18.
- 159 B. Lee, H. R. Lee, H. Kim, K. Y. Chung, B. W. Cho and S. H. Oh, *Chem. Commun.*, 2015, **51**, 9265-9268.
- 160 M. H. Alfaruqi, V. Mathew, J. Gim, S. Kim, J. Song, J. P. Baboo, S. H. Choi and J. Kim, *Chem. Mater.*, 2015, **27**, 3609-3620.
- 161 A. M. Tripathi, W.-N. Su and B. J. Hwang, *Chem. Soc. Rev.*, 2018, **47**, 736-851.
- 162 D. Liu, Z. Shadike, R. Lin, K. Qian, H. Li, K. Li, S. Wang, Q. Yu, M. Liu, S. Ganapathy, X. Qin, Q.-H. Yang, M. Wagemaker, F. Kang, X.-Q. Yang and B. Li, *Adv. Mater.*, 2019, **31**, 1806620.
- 163 P. Kumar, E. W. Zaia, E. Yildirim, D. V. M. Repaka, S.-W. Yang, J. J. Urban and K. Hippalgaonkar, *Nat. Commun.*, 2018, **9**, 5347.
- 164 P. Raccuglia, K. C. Elbert, P. D. F. Adler, C. Falk, M. B. Wenny, A. Mollo, M. Zeller, S. A. Friedler, J. Schrier and A. J. Norquist, *Nature*, 2016, **533**, 73-76.
- 165 L. Xi, S. Pan, X. Li, Y. Xu, J. Ni, X. Sun, J. Yang, J. Luo, J. Xi, W. Zhu, X. Li, D. Jiang, R. Dronskowski, X. Shi, G. J. Snyder and W. Zhang, *J. Am. Chem. Soc.*, 2018, **140**, 10785-10793.
- 166 J. Schmidt, Mário R. G. Marques, Silvana Botti & Miguel A. L. Marques, *npj Comput. Mater.*, 2019, **5**, 83.

ToC



Recent progress on 2D organic-inorganic superlattices by alternate stacking of organic layers and inorganic sheets is reviewed.

Broader context

Two-dimensional (2D) heterostructures or superlattices, assembled by vertical stacking of 2D materials on top of each other, are a new class of artificial 2D materials of significant scientific and technological importance. Numerous unconventional properties have been demonstrated when different 2D nanosheets are combined at a molecular scale. Compared to inorganic materials, an almost unlimited number of organic materials could be potentially available with designed functional groups. Therefore, introduction of the chemical tunability of 2D organic molecules/polymers within the 2D heterostructures/superlattices provides unlimited possibilities for the design of 2D organic-inorganic superlattices with predictable functionalities. Herein, we review recent research progress on 2D organic-inorganic superlattice-like heterostructures, in which continuous organic layers are intercalated in the interlayer galleries of inorganic 2D nanosheets at an atomic/molecular scale. We systematically summarize four facile synthesis strategies and discuss the advantages of these 2D superlattices for some typical energy storage applications. In addition, the challenges and perspectives for future researches are also highlighted. We believe that this summary may open up new opportunities for artificial design of 2D heterostructures or superlattices with desired properties and functionalities at an atomic/molecular level.